Available online at www.sciencedirect.com
ScienceDirect
Journal of Sound and Vibration 314 (2008) 712–737
JOURNAL OF SOUND AND VIBRATION
www.elsevier.com/locate/jsvi

A boundary integral formulation for sound scattered by elastic moving bodies

M. Gennaretti[a,*], C. Testa[b]

[a]Department of Mechanical and Industrial Engineering, University Roma Tre, Via della Vasca Navale 79, 00146 Rome, Italy
[b]INSEAN, Italian Ship Model Basin, Via di Vallerano 139, 00128 Rome, Italy

Received 29 June 2006; received in revised form 14 January 2008; accepted 15 January 2008
Handling Editor: C. Morfey
Available online 7 March 2008

Abstract

This paper deals with the acoustic field scattered by elastic bodies in motion. Starting from the Ffowcs Williams and Hawkings equation for porous surfaces, a boundary integral formulation for the acoustic disturbance is derived. For moving, vibrating bodies impinged by acoustic waves it yields a unified approach for the determination of surface pressure perturbations and sound radiation. The scattered field is determined from the knowledge of the impinging pressure, without requiring the evaluation of its normal derivative over the surface of the scatterer. A boundary element method is applied for the numerical solution of the integral formulation. The resulting prediction tool is validated through acoustic analysis of stationary rigid and elastic spherical shells, as well as a wing and a vibrating sphere in uniform motion. The advantages of the proposed sound scattering formulation are discussed.

1. Introduction

The aim of this work is to evaluate the acoustic field generated by pressure waves scattered by moving, elastic bodies. The problem of sound scattering is present in a wide range of engineering applications dealing with steady and moving objects. In aeronautics, for instance, the evaluation of scattered acoustic fields is of interest both for the evaluation of overall noise emitted by moving aircraft and for the prediction of fuselage wall vibrations that, in turn, are a source of cabin noise (aeroacoustoelastic application). The decomposition of the noise field into incident and scattered components is useful when, within the limits of the required accuracy, the source of the incident field may be considered independent of the presence of the scattering surface. Indeed, in aeronautical applications where the main source of noise is an aircraft component that may be assumed to be aerodynamically independent, first the incident pressure field may be determined through an aerodynamic/aeroacoustic analysis of it, and then the rest of the aircraft configuration (the scattering portion) may be taken into account in the second step of the process dealing with the scattered field. For instance, this approach is applicable in the analysis of propeller-driven aircraft where the noise emitted by the propellers is

*Corresponding author. Tel.: +39 06 57333260; fax: +39 06 5593732.
E-mail address: m.gennaretti@uniroma3.it (M. Gennaretti).

0022-460X/$ - see front matter © 2008 Elsevier Ltd. All rights reserved.
doi:10.1016/j.jsv.2008.01.028

scattered by the fuselage [1]. However, a similar acoustic analysis may also be applied to those rotorcraft configurations where the rotating blades are the main source of noise, with the major contribution of the fuselage to the noise field being represented by its scattering effect (some helicopter flight configurations fall within this category) [2].

The analysis of noise scattering involves pressure waves impinging both on non-moving and on moving surfaces. A wide literature is available on this subject (see, for instance, Refs. [3–12]). It includes works dealing with the discussion of techniques for the regularization of the scattered field that is needed when fictitious eigenfrequencies appear in the integral operator governing the problem (see, for instance, Ref. [4] for a review on this issue).

Here, the pressure field scattered by an elastic moving body is analyzed through a boundary integral formulation based on the Ffowcs Williams and Hawkings (FW-H) equation [13]. This formulation, that extends and improves the one presented in Ref. [14], yields a unified solver that is not only able to radiate the sound, but can also be used to evaluate the acoustic disturbance over moving, vibrating surfaces. It may be conveniently applied to acoustoelastic problems where body elastic vibrations interact with the exterior pressure field and generate noise within its cavity (if any). For aeronautical applications, sound radiation prediction tools derived from the FW-H equation have been proven to be very efficient. They are able to evaluate both the noise due to the pressure distribution over the body (loading noise) and that given by air perturbation produced by the body motion (thickness noise). The analysis of sound scattering is not a standard field of application of the FW-H equation, and this issue has recently been discussed in some papers [15–18]. However, it is shown that the resulting boundary integral formulation derived from it is able to predict near-field and far-field scattered solutions, also showing some advantages in terms of numerical application simplicity. In particular, the scattered field is obtained from the knowledge of the incident field over the surfaces of the scatterers, instead of requiring the evaluation of its normal derivative, as it is in widely used integral approaches for sound scattering analysis (like, for instance, those based on the Kirchhoff integral operator).

The acoustic formulation introduced is validated by comparisons with analytical solutions for rigid and elastic spheres impinged by plane pressure waves. Problems of sound scattered by a wing in uniform rectilinear motion and of sound generated by a vibrating moving sphere are also examined.

2. A boundary integral formulation for the acoustic disturbance from porous surfaces

Prediction tools based on the FW-H equation [13] have been proven to be very efficient aeroacoustic solvers in aeronautical subsonic and supersonic configurations, where the sound generated aerodynamically plays a significant role. Here, the FW-H equation is applied for the development of a methodology aimed at the analysis of sound scattered by elastic vibrating surfaces. This approach is outlined in the next sections and is based on the boundary integral formulation for the solution of the FW-H equation described in the following.

Let us assume that the fluid is compressible and undergoes transformations with negligible entropy changes. If N bodies move in the fluid, each having velocity $\mathbf{v}_j$ in a frame of reference fixed to the undisturbed medium (air frame), and a permeable (porous) boundary surface S_j defined by those points that satisfy $f_j(\mathbf{x},t)=0$, the following form of the FW-H equation [13] can be obtained (see also Refs. [19,20]):

$$\begin{aligned}\Box^2 p' = &\sum_j^N \frac{\overline{\partial}}{\partial t}[\rho_0 \mathbf{v}_j\cdot\nabla f_j \delta(f_j)] + \frac{\overline{\partial}}{\partial t}[\rho(\mathbf{u}-\mathbf{v}_j)\cdot\nabla f_j\delta(f_j)]\\ &-\sum_j^N \overline{\nabla}\cdot[\mathbf{P}\nabla f_j\delta(f_j)] - \sum_j^N \overline{\nabla}\cdot[\rho\mathbf{u}(\mathbf{u}-\mathbf{v}_j)\cdot\nabla f_j\delta(f_j)]\\ &+\overline{\nabla}\cdot\left\{\overline{\nabla}\cdot\left[\mathbf{T}\prod_j^N H(f_j)\right]\right\}, \quad \forall \mathbf{x}\in\Re^3,\end{aligned} \tag{1}$$

where $p'=c^2\hat{\rho}$ is the acoustic disturbance, with $\hat{\rho}=(\rho-\rho_0)$ representing the density perturbation and c and ρ_0 denoting, respectively, the speed of sound and the density of the undisturbed medium. The bars denote

generalized differential operators and $\overline{\Box}^2 = (1/c^2)(\overline{\partial}^2/\partial t^2) - \overline{\nabla}^2$ is the generalized wave operator. In addition, $\mathbf{P} = (p - p_0)\mathbf{I} = \hat{p}\mathbf{I}$ and $\mathbf{T} = \rho\mathbf{u} \otimes \mathbf{u} + (\hat{p} - c^2\hat{\rho})\mathbf{I}$ denote, respectively, the compressive stress tensor and the Lighthill tensor, $\mathbf{u}$ is the fluid velocity in the air frame of reference, whereas H and δ are Heaviside and Dirac delta functions. The two terms where the difference $(\mathbf{u} - \mathbf{v}_j)$ between the fluid and the surface velocity appears are those arising only in case of porous boundary surfaces.

Following the theoretical approach introduced in Ref. [21] and extended to more complex subsonic aeronautical configurations in Ref. [22], assuming the nonlinear perturbation field terms to be negligible and the body surfaces to be rigid, for f_j such that $|\nabla f_j| = 1$, the boundary integral representation of the acoustic field governed by Eq. (1) is given by

$$\begin{aligned} p'(\mathbf{x},t) = & -\sum_j^N \int_{S_j} \rho_0[\mathbf{v}\cdot\mathbf{n}\mathbf{v}\cdot\nabla\hat{G} + [\mathbf{v}\cdot\mathbf{n}(1-\mathbf{v}\cdot\nabla\theta)]^{\cdot}\hat{G}]_{\mathrm{ret}}\,\mathrm{d}S \\ & -\sum_j^N \int_{S_j} [(\mathbf{P}\mathbf{n})\cdot\nabla\hat{G} - (\dot{\mathbf{P}}\mathbf{n})\cdot\nabla\theta\hat{G}]_{\mathrm{ret}}\,\mathrm{d}S \\ & -\sum_j^N \int_{S_j} [\rho\mathbf{u}^-\cdot\mathbf{n}\mathbf{u}^+\cdot\nabla\hat{G} + [\rho\mathbf{u}^-\cdot\mathbf{n}(1-\mathbf{u}^+\cdot\nabla\theta)]^{\cdot}\hat{G}]_{\mathrm{ret}}\,\mathrm{d}S, \end{aligned} \tag{2}$$

where each moving surface is defined in a Lagrangean frame, $\boldsymbol{\eta}$, fixed to the surface (i.e., the integrations are performed over time-independent surfaces). In the equation above, $\mathbf{u}^- = (\mathbf{u} - \mathbf{v}), \mathbf{u}^+ = (\mathbf{u} + \mathbf{v})$, $\mathbf{n}$ denotes the outward unit normal on S_j, whereas

$$\hat{G}(\mathbf{x},\boldsymbol{\eta},t) = \frac{-1}{4\pi}\left[\frac{1}{r(1-M_r)}\right]_{\mathrm{ret}},$$

where, for $(\mathbf{x},t)$ and $(\mathbf{y},\tau)$ representing, respectively, observer and source space–time variables in the air frame, $r = |\mathbf{r}| = |\mathbf{x} - \mathbf{y}(\boldsymbol{\eta},\tau)|$, while $(1 - M_r)$ is the Doppler factor with $M_r = \mathbf{v}\cdot(\mathbf{r}/r)/c$ denoting the surface velocity Mach number in the direction of radiation. In addition, the symbol $(\dot{})$ denotes the time derivative keeping fixed a surface point, whereas the symbol $[\,]_{\mathrm{ret}}$ indicates that the quantities must be evaluated at the retarded emission time, $\tau_e = t - \theta$, where θ is the time taken by an acoustic disturbance released from a surface source point, $\boldsymbol{\eta}$, to reach the observer location, $\mathbf{x}$, at current time, t. The time delay, θ, is evaluated as root of the equation $|\mathbf{x} - \mathbf{y}(\boldsymbol{\eta}, t-\theta)|/c - \theta = 0$. Note that the integrands appearing in Eq. (2) have to be interpreted carefully. In particular, when for computational application the analytical gradients of $\hat{G}$ and θ are carried out, attention has to be paid to the variables they depend on (see, for instance, Refs. [21–24] where some critical issues concerning this kind of integral formulations are discussed).

Integral representations of the solution of the FW-H equation of the type in Eq. (2) are commonly applied in aeroacoustics to compute the noise radiated by moving impermeable bodies ($\mathbf{u}^- \cdot \mathbf{n} = 0$), once the pressure distributions over their boundary surfaces are known from an aerodynamic solver. As already mentioned above, here the intended application of Eq. (2) is to derive an integral equation to compute the pressure perturbation over vibrating surfaces impinged by pressure waves and the corresponding noise radiated (elastic body scattering). It is possible to demonstrate that, under the body impermeability assumption, the integral formulation in Eq. (2) is exactly equivalent to Farassat's Formulation 1A [24–26], with the first integral representing the thickness noise and the second one the loading noise. The third integral takes into account the modifications to the acoustic radiation from moving bodies due to surface porosity effects.

The extension of the integral formulation presented above to deformable bodies may be achieved following the approach presented in Refs. [27,23].

3. Acoustic disturbance in the presence of impinging pressure waves

The analysis of the noise radiated by bodies that are impinged by pressure waves is of interest in many acoustic applications, with inclusion of environmental noise detection. It concerns acoustic configurations where a noise source distribution radiates a pressure disturbance (incident) field that, interacting with moving

or stationary bodies, is subject to modifications in directivity and intensity (scattering effects). An essential feature of this kind of problems is that the noise source is assumed to be independent of the presence of scatterers.

Thus, in order to analyze the problem of pressure waves impinging on moving bodies through the formulation in Section 2, let us assume that two surfaces are present in the domain of interest: one, S_B, is the boundary of an arbitrarily moving scattering body, whereas the second, S_I, is a closed surface that surrounds the sources of an incident acoustic disturbance. The limitation of the analysis to one single scattering body is for the sake of simplicity, and does not affect the generality of the formulation that will be developed. The surface S_I is a virtual, arbitrarily shaped surface that is perfectly permeable and does not alter the flow field (it is introduced only to derive the integral formulation for the scattered field). The only constraint in its choice is that it must be close enough to the sources of the pressure disturbances (moving with them, if necessary) in such a way that the flow field over it is unaffected by the presence of the scattering body. Under these assumptions, noting that acoustic disturbance and pressure perturbation coincide under the hypothesis of small perturbation fields, the incident pressure distribution, p'_I, may be expressed by the following integral representation for $\mathbf{x}$ outside S_I [Eq. (2) written for 'frozen' noise sources]:

$$\begin{aligned} p'_I(\mathbf{x},t) = & -\int_{S_I} \rho_0[\mathbf{v}\cdot\mathbf{n}\mathbf{v}\cdot\nabla\hat{G} + [\mathbf{v}\cdot\mathbf{n}(1-\mathbf{v}\cdot\nabla\theta)]\dot{}\,\hat{G}]_{\mathrm{ret}}\,\mathrm{d}S \\ & -\int_{S_I} [p'_I\mathbf{n}\cdot\nabla\hat{G} - \dot{p}'_I\mathbf{n}\cdot\nabla\theta\hat{G}]_{\mathrm{ret}}\,\mathrm{d}S \\ & -\int_{S_I} [\rho\mathbf{u}_I^-\cdot\mathbf{n}\mathbf{u}_I^+\cdot\nabla\hat{G} + [\rho\mathbf{u}_I^-\cdot\mathbf{n}(1-\mathbf{u}_I^+\cdot\nabla\theta)]\dot{}\,\hat{G}]_{\mathrm{ret}}\,\mathrm{d}S, \end{aligned} \tag{3}$$

where the porosity effects are due to the velocity field, $\mathbf{u}_I$, related to the incident pressure. Then, decomposing the total acoustic disturbance field into the incident component and the component, p'_B, due to the body presence (i.e., for $p' = p'_B + p'_I$), the combination of Eq. (2) for $\mathbf{x}$ outside S_B (and S_I) with Eq. (3) yields the following boundary integral representation for the acoustic disturbance due to the body impinged by the incident pressure wave

$$\begin{aligned} p'_B(\mathbf{x},t) = & -\int_{S_B} \rho_0[\mathbf{v}\cdot\mathbf{n}\mathbf{v}\cdot\nabla\hat{G} + [\mathbf{v}\cdot\mathbf{n}(1-\mathbf{v}\cdot\nabla\theta)]\dot{}\,\hat{G}]_{\mathrm{ret}}\,\mathrm{d}S \\ & -\int_{S_B} [p'_B\mathbf{n}\cdot\nabla\hat{G} - \dot{p}'_B\mathbf{n}\cdot\nabla\theta\hat{G}]_{\mathrm{ret}}\,\mathrm{d}S \\ & -\int_{S_B} [p'_I\mathbf{n}\cdot\nabla\hat{G} - \dot{p}'_I\mathbf{n}\cdot\nabla\theta\hat{G}]_{\mathrm{ret}}\,\mathrm{d}S \\ & -\int_{S_B} [\rho\mathbf{u}^-\cdot\mathbf{n}\mathbf{u}^+\cdot\nabla\hat{G} + [\rho\mathbf{u}^-\cdot\mathbf{n}(1-\mathbf{u}^+\cdot\nabla\theta)]\dot{}\,\hat{G}]_{\mathrm{ret}}\,\mathrm{d}S. \end{aligned} \tag{4}$$

This equation may be applied to determine the noise radiated by the body once p'_B is evaluated over its surface. For this purpose, the equation above may be written for $\mathbf{x}\in S_B$, thus yielding the following boundary integral equation:

$$\begin{aligned} [1-\lambda(\mathbf{x},t)]p'_B(\mathbf{x},t) = & \lambda(\mathbf{x},t)[\rho_0 v_n^2(\mathbf{x},t) + p'_I(\mathbf{x},t) + \rho u_n^-(\mathbf{x},t)u_n^+(\mathbf{x},t)] \\ & -\int_{S_B} \rho_0[\mathbf{v}\cdot\mathbf{n}\mathbf{v}\cdot\nabla\hat{G} + [\mathbf{v}\cdot\mathbf{n}(1-\mathbf{v}\cdot\nabla\theta)]\dot{}\,\hat{G}]_{\mathrm{ret}}\,\mathrm{d}S \\ & -\int_{S_B} [p'_B\mathbf{n}\cdot\nabla\hat{G} - \dot{p}'_B\mathbf{n}\cdot\nabla\theta\hat{G}]_{\mathrm{ret}}\,\mathrm{d}S \\ & -\int_{S_B} [p'_I\mathbf{n}\cdot\nabla\hat{G} - \dot{p}'_I\mathbf{n}\cdot\nabla\theta\hat{G}]_{\mathrm{ret}}\,\mathrm{d}S \\ & -\int_{S_B} [\rho\mathbf{u}^-\cdot\mathbf{n}\mathbf{u}^+\cdot\nabla\hat{G} + [\rho\mathbf{u}^-\cdot\mathbf{n}(1-\mathbf{u}^+\cdot\nabla\theta)]\dot{}\,\hat{G}]_{\mathrm{ret}}\,\mathrm{d}S, \end{aligned} \tag{5}$$

where $v_n = \mathbf{v}\cdot\mathbf{n}$, $u_n^- = \mathbf{u}^-\cdot\mathbf{n}$, $u_n^+ = \mathbf{u}^+\cdot\mathbf{n}$ and $\lambda = 0.5/(1-M_n^2)$, with $M_n = v_n/c$. Eq. (5) is a boundary integral equation through which p'_B may be determined on S_B from the knowledge of incident pressure field, motion of the body and porosity effects. The additional terms related to the coefficient λ that are evaluated at the observer position come from the singularities of the kernel function, $\nabla\hat{G}$, arising for $\mathbf{x}\in S_B$ (see Appendix A for details on their derivation and on the corresponding interpretation of the integrals over S_B); some of these terms coincide with those introduced by Long [28] for aerodynamic applications of Formulation 1A by Farassat.

The acoustic formulation represented by Eqs. (4) and (5) yields the sound radiated by the body with the only requirement of knowing incident pressure field, body motion and the nature of porosity contributions (usually of small perturbation type and related to body surface characteristics). In the presence of multiple bodies, this formulation, when extended to the whole set of bodies, is able to also capture the interactional effects. An acoustics approach of this type could be of interest, for instance, in the prediction of the noise produced by those aeronautical multibody configurations where, within the limits of the required accuracy, it is possible to identify one single body as the main noise source, with the pressure on it approximately independent of the presence of the other bodies. Indeed, in this case, the only aerodynamic input required would be that related to the pressure solution on the isolated noise source body to be used in Eq. (3) for the determination of the incident pressure field (propeller-driven aircraft could be an example of such aeronautical configurations).

4. Sound radiated by scattering and vibrating surfaces

Observing Eqs. (4) and (5), it is evident that the pressure field over an arbitrarily moving body, along with the noise it radiates, is the result of the action of three forcing terms: one is related to the rigid-body motion, one is related to the impinging pressure wave and one is related to the surface porosity.

The formulation presented above is not intended for the prediction of pressure perturbation generated by rigid-body motion (neither for lifting nor for non-lifting configurations). Pressure perturbations over arbitrarily shaped bodies that are caused by rigid-body motion usually correspond to non-small velocity perturbations, and thus their accurate evaluation would require the inclusion of the contribution from the Lighthill tensor in Eq. (1) (see, for instance, Refs. [29,30] for the analysis of the quadrupole terms). This problem does not occur in the standard aeroacoustics since the pressure over the surface is obtained from an aerodynamic solver and the inaccuracy mentioned above disappears when the acoustic disturbance is evaluated at points that are far from the emitting surface (see the quadrupole expression in Refs. [29,30]). In addition, note that in many sound-scattering applications, if not stationary, the scatterer motion is a uniform translation that yields a constant pressure field over the body surface and does not produce any noise disturbance at points located in a frame of reference fixed with it.

The present formulation is aimed at the prediction of the acoustic disturbance generated by elastic shells when impinged by pressure waves, i.e., due to pressure perturbations from scattering and surface vibration effects. Surface vibration effects may be simulated as surface porosity contributions. Indeed, because of body impenetrability, surface vibrations produce a difference between the normal component of the rigid-body velocity and that of the fluid flow, and it corresponds exactly to the 'elastic transpiration velocity' term $\chi = \mathbf{u}^-\cdot\mathbf{n} \equiv (\mathbf{u}-\mathbf{v})\cdot\mathbf{n}$ which represents surface porosity effects in Eqs. (1), (4) and (5). Note that this is the only way to include theoretically the influence of wall vibrations in an integral formulation that has been derived under the assumption of rigid surfaces, without arbitrarily introducing approximated effects related to (not compatible) surface deformations.

Then, let us decompose the pressure perturbation field into a component due to the rigid-body motion, p'_R, and a scattering component, p'_S, due to incident pressure and surface vibrations, such that $p'_B = p'_R + p'_S$. Because of the linearity of the integral operator introduced above, it is possible to derive an integral equation for p'_R forced by the terms involving the rigid-body motion velocity (thickness-noise terms), and an integral equation for p'_S forced by incident pressure and surface vibrations. In particular, assuming that the elastic transpiration velocity is a small-perturbation term and discarding the second-order perturbation terms from the surface porosity contribution, Eq. (5) yields the following boundary integral equation for the sound

scattered by a moving, vibrating surface:

$$
\begin{aligned}
[1-\lambda(\mathbf{x},t)]p'_S(\mathbf{x},t) = {} & \lambda(\mathbf{x},t)[p'_I(\mathbf{x},t)+2\rho_0 v_n \chi(\mathbf{x},t)] \\
& - \int_{S_B} [p'_S \mathbf{n}\cdot\nabla\hat{G} - \dot{p}'_S \mathbf{n}\cdot\nabla\theta\hat{G}]_{\mathrm{ret}}\,\mathrm{d}S \\
& - \int_{S_B} [p'_I \mathbf{n}\cdot\nabla\hat{G} - \dot{p}'_I \mathbf{n}\cdot\nabla\theta\hat{G}]_{\mathrm{ret}}\,\mathrm{d}S \\
& - \int_{S_B} \rho_0[\chi(\mathbf{u}_0+\mathbf{v})\cdot\nabla\hat{G} + [\chi(1-(\mathbf{u}_0+\mathbf{v})\cdot\nabla\theta)]^{\cdot}\hat{G}]_{\mathrm{ret}}\,\mathrm{d}S,
\end{aligned}
\tag{6}
$$

where $\mathbf{u}_0$ is the fluid velocity over the unperturbed body (note that $\mathbf{u}_0\cdot\mathbf{n} = \mathbf{v}\cdot\mathbf{n}$ in the unperturbed, nonvibrating, impermeable body configuration). This boundary integral equation yields the scattered pressure from the knowledge of the incident pressure over the surface and surface elastic vibrations. Once p'_S is known on the body surface, the corresponding integral representation derived from Eq. (4) may be applied to determine p'_S in the field. Note that, although the rigid-body motion pressure perturbation, p'_R, is not present in this formulation (as motivated above), the effects of rigid-body oscillations (if any) can always be taken into account through the transpiration velocity term. The inclusion of the vibrational effects allows the application of the acoustic formulation presented in acoustoelastic problems where wall vibrations transmit exterior pressure disturbances within the cavity bounded by the deforming wall (typical aircraft cabin noise production mechanism). The acoustic formulation presented is a simplification with respect to widely used scattering formulations that require knowledge of the normal derivative of the incident pressure over the scatterer surface. It is either directly applied as a boundary condition (formulations based on the Kirchhoff integral operator), or used to determine the normal acoustic velocity appearing in the impenetrability surface condition. Indeed, whenever the incident pressure field is the result of complex acoustic radiation processes (like, for instance, those occurring in aeronautical problems involving helicopter rotors and propellers), the numerical evaluation of the pressure gradient may become computationally expensive in terms of run time and memory use and introduce further approximation in the algorithm of solution. Recently, some authors have developed a boundary integral formulation for the computationally efficient evaluation of the pressure gradient, starting from Farassat's Formulation 1A [31].

Scattering, vibroacoustic problems are usually analyzed in the frequency domain, where the acoustic field is evaluated for each harmonic of the incident wave pressure and of the vibrating motion. Because of the linearity of Eq. (6), if the body velocity has constant components in a body-fixed frame of reference so that all terms are time independent (of course, with the exception of p'_I, p'_S and χ), then it is possible to transform it in the frequency domain. For $p'(\mathbf{x},t) = \tilde{p}'(\mathbf{x},\omega)\,\mathrm{e}^{\mathrm{i}\omega t}$ and $\chi(\mathbf{x},t) = \tilde{\chi}(\mathbf{x},\omega)\,\mathrm{e}^{\mathrm{i}\omega t}$ this yields

$$
\begin{aligned}
[1-\lambda(\mathbf{x})]\tilde{p}'_S(\mathbf{x},k) = {} & \lambda(\mathbf{x})[\tilde{p}'_I(\mathbf{x},k)+2\rho_0 c M_n \tilde{\chi}(\mathbf{x},k)] \\
& - \int_{S_B} [\mathbf{n}\cdot\nabla\hat{G} - \mathrm{i}k\mathbf{n}\cdot\nabla\sigma\hat{G}]\tilde{p}'_S(\mathbf{y},k)\,\mathrm{e}^{-\mathrm{i}k\sigma}\,\mathrm{d}S \\
& - \int_{S_B} [\mathbf{n}\cdot\nabla\hat{G} - \mathrm{i}k\mathbf{n}\cdot\nabla\sigma\hat{G}]\tilde{p}'_I(\mathbf{y},k)\,\mathrm{e}^{-\mathrm{i}k\sigma}\,\mathrm{d}S \\
& - \int_{S_B} \rho_0 c[\hat{\mathbf{M}}\cdot\nabla\hat{G} + \mathrm{i}k(1-\hat{\mathbf{M}}\cdot\nabla\sigma)\hat{G}]\tilde{\chi}(\mathbf{y},k)\,\mathrm{e}^{-\mathrm{i}k\sigma}\,\mathrm{d}S,
\end{aligned}
\tag{7}
$$

where $k = \omega/c$ is the wave number, $\sigma = c\theta$, $M_n = v_n/c$ and $\hat{\mathbf{M}} = (\mathbf{u}_0+\mathbf{v})/c$.

Once the pressure over the scattering, vibrating surface has been evaluated by Eq. (7), the following boundary integral representation gives the corresponding acoustic disturbance it radiates in the field:

$$
\begin{aligned}
\tilde{p}'_S(\mathbf{x},k) = {} & - \int_{S_B} [\mathbf{n}\cdot\nabla\hat{G} - \mathrm{i}k\mathbf{n}\cdot\nabla\sigma\hat{G}]\tilde{p}'_S(\mathbf{y},k)\,\mathrm{e}^{-\mathrm{i}k\sigma}\,\mathrm{d}S \\
& - \int_{S_B} [\mathbf{n}\cdot\nabla\hat{G} - \mathrm{i}k\mathbf{n}\cdot\nabla\sigma\hat{G}]\tilde{p}'_I(\mathbf{y},k)\,\mathrm{e}^{-\mathrm{i}k\sigma}\,\mathrm{d}S \\
& - \int_{S_B} \rho_0 c[\hat{\mathbf{M}}\cdot\nabla\hat{G} + \mathrm{i}k(1-\hat{\mathbf{M}}\cdot\nabla\sigma)\hat{G}]\tilde{\chi}(\mathbf{y},k)\,\mathrm{e}^{-\mathrm{i}k\sigma}\,\mathrm{d}S.
\end{aligned}
\tag{8}
$$

Hence, the procedure proposed in this work to determine the frequency-domain acoustic field generated by a scattering, vibrating surface consists of the following three steps: first, the incident pressure is evaluated over the surface, then the integral equation Eq. (7) is applied to determine the pressure perturbation over the surface and finally the integral representation Eq. (8) is used to evaluate the acoustic disturbance in the field.

5. Numerical results

The numerical investigation is performed by applying a zeroth-order boundary element method for the discretization of the boundary integral formulation. It consists of dividing the scattering and vibrating surface, S_B, into quadrilateral panels and assuming $\tilde{p}'_S$, $\tilde{p}'_I$ and $\tilde{\chi}$ to be piecewise constant. Then, the integral equation is solved by requiring that the equation be satisfied at the center of each body element (collocation method, see also Ref. [22]). Specifically, discretizing S_B into M panels, S_m^B, for a given value of k, at the center of the jth element, $\mathbf{x}_j$, Eq. (7) yields

$$\begin{aligned}(1-\lambda_j)\tilde{p}_j^S(k) = &\sum_{m=1}^{M}(B_{jm}+\mathrm{i}kC_{jm})\tilde{p}_m^S(k)\\ &+\sum_{m=1}^{M}(\lambda_m\delta_{jm}+B_{jm}+\mathrm{i}kC_{jm})\tilde{p}_m^I(k)\\ &+\sum_{m=1}^{M}(2M_m^n\lambda_m\delta_{jm}+D_{jm}+\mathrm{i}kF_{jm})\tilde{\chi}_m(k),\end{aligned} \tag{9}$$

where $\tilde{p}_j^S(k)=\tilde{p}'_s(\mathbf{x}_j,k)$, while $\tilde{p}_m^S(k)=\tilde{p}'_s(\mathbf{x}_m,k)$, $\tilde{p}_m^I(k)=\tilde{p}'_i(\mathbf{x}_m,k)$, $\tilde{\chi}_m(k)=\tilde{\chi}(\mathbf{x}_m,k)/\rho_0 c$, $M_m^n=M_n(\mathbf{x}_m)$ and $\lambda_m=\lambda(\mathbf{x}_m)$, with $\mathbf{x}_m$ denoting the center of the mth panel. In addition, δ_{jm} is the Kronecher delta function and the coefficients are defined in the following way:

$$\begin{aligned}B_{jm}(k) &= -\mathrm{e}^{-\mathrm{i}k\sigma_{jm}}\int_{S_m^B}\mathbf{n}\cdot\nabla\hat{G}\,\mathrm{d}S,\\ C_{jm}(k) &= \mathrm{e}^{-\mathrm{i}k\sigma_{jm}}\int_{S_m^B}\mathbf{n}\cdot\nabla\sigma\hat{G}\,\mathrm{d}S,\\ D_{jm}(k) &= -\mathrm{e}^{-\mathrm{i}k\sigma_{jm}}\int_{S_m^B}\hat{\mathbf{M}}\cdot\nabla\hat{G}\,\mathrm{d}S,\\ F_{jm}(k) &= -\mathrm{e}^{-\mathrm{i}k\sigma_{jm}}\int_{S_m^B}(1-\hat{\mathbf{M}}\cdot\nabla\sigma)\hat{G}\,\mathrm{d}S\end{aligned}$$

with σ_{jm} denoting the time delay of the propagation of signals between the source point at $\mathbf{x}_m$ and the observer point at $\mathbf{x}_j$ [a similar procedure is used for the numerical application of Eq. (8) to evaluate the acoustic disturbance in the field]. Note that in the numerical evaluation of the above coefficients, the gradients of $\hat{G}$ and σ are first carried out analytically (see, for instance, Refs. [21–23]), and then the corresponding expressions given in terms of source and observer positions are integrated assuming a hyperboloidal panel shape.

Collecting scattered pressures, incident pressures and elastic transpiration velocities at the M panels in the vectors p_S, p_I and x, respectively, and collecting the coefficients in the matrices $\mathsf{B}, \mathsf{C}, \mathsf{D}$ and F, the solution of Eq. (9) may be written in the following matrix form:

$$\tilde{\mathsf{p}}_S = \mathsf{E}_I(k)\tilde{\mathsf{p}}_I + \mathsf{E}_\chi(k)\tilde{\mathsf{x}}, \tag{10}$$

where, for I denoting the unit matrix and Λ denoting the diagonal matrix collecting the λ_m's,

$$\mathsf{E}_I(k) = [\mathsf{I}-\Lambda-\mathsf{B}(k)-\mathrm{i}k\mathsf{C}(k)]^{-1}[\Lambda+\mathsf{B}(k)+\mathrm{i}k\mathsf{F}(k)] \tag{11}$$

is the matrix of the transfer functions between incident and scattered pressures at the panel centers, while

$$\mathsf{E}_\chi(k) = [\mathsf{I}-\Lambda-\mathsf{B}(k)-\mathrm{i}k\mathsf{C}(k)]^{-1}[2\mathsf{M}\Lambda+\mathsf{D}(k)+\mathrm{i}k\mathsf{F}(k)] \tag{12}$$

is the matrix of the transfer functions between elastic vibrations and pressure perturbations, with M denoting the diagonal matrix collecting the normal Mach numbers, M_m^n's.

In order to validate the acoustic formulation presented, first, results concerning the pressure field generated by a plane wave impinging on a stationary rigid sphere are presented and compared with available analytical solutions. The problem of the appearance of spurious frequencies is examined, along with acoustically small sphere configurations. Then, the surface deformation effects on sound scattered are analyzed by assuming that the sphere is a thin elastic shell subject to vibrations because of the impinging plane pressure wave. Also in this case, the numerical predictions are validated by comparison with analytical solutions. Finally, the acoustic analysis of scattering and vibrating surfaces is performed for bodies in uniform rectilinear motion, and the results are compared with those given by a formulation based on the velocity potential.

5.1. Plane wave scattered by a stationary rigid sphere

The solution of the problem of a plane wave impinging on a stationary rigid sphere is obtained through the application of the boundary integral equation in Eq. (7), with $\mathbf{v} = \mathbf{0}$, $\tilde{\chi} = 0$ and $\tilde{p}'_I(x,k) = \mathrm{e}^{-\mathrm{i}kx}$ (the wave is assumed to propagate along the x-axis). In Appendix B it is shown that, in this case, the present boundary integral formulation for the scattered pressure becomes perfectly equivalent to that discussed in Ref. [17] for the same kind of problem. The formulation in Ref. [17] has been obtained starting from the FW-H equation written only for the scattered pressure.

For a sphere of radius R, and an impinging wave with wave number such that $kR = 1$, Fig. 1 depicts the comparison between the analytical scattered pressure solution [32, p. 419, Eq. (8.2.2)] and those obtained numerically using an increasing number of panels to discretize the sphere surface. The scattered signal is evaluated on a circle of radius $d/R = 5$ centered at the center of the sphere; N_m denotes the number of elements of discretization along its meridians and N_p denotes the number of elements of discretization along the parallel circles (the x-axis coincides with the polar axis). The result is given in terms of the angular dependence of the ratio $|\tilde{p}'_S|/|\tilde{p}'_I|$, for the impinging wave traveling from left to right. The same will be done for all of the following figures, unless different definitions are specifically indicated. For $N_m = N_p = 32$ the

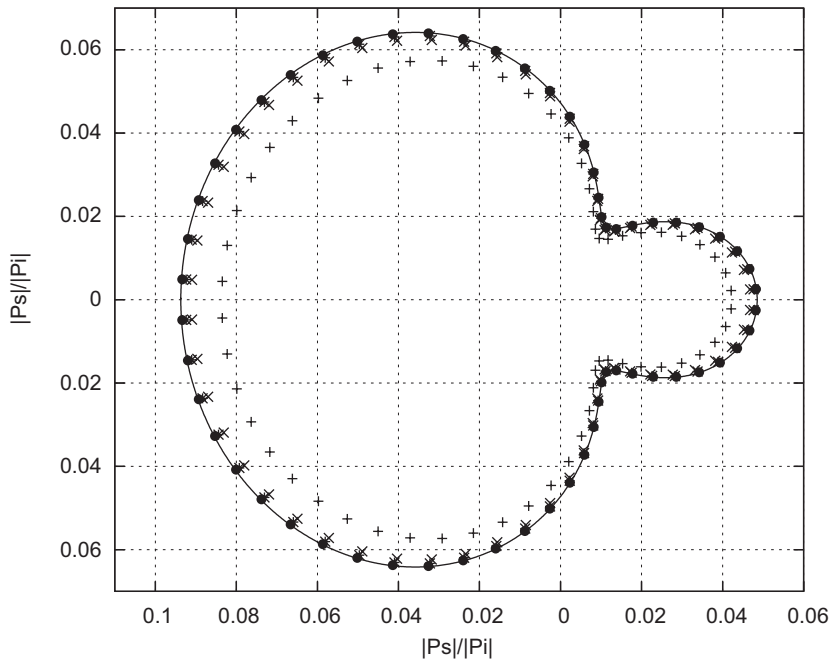

Fig. 1. Angular dependence of scattering for a plane wave impinging on a stationary sphere. Convergence analysis and comparison with the analytical solution for $kR = 1$ and $d/R = 5$. —, analytical solution; +, $N_m = N_p = 8$; ×, $N_m = N_p = 16$; ✻, $N_m = N_p = 24$; •, $N_m = N_p = 32$ (the incident wave moves from left to right).

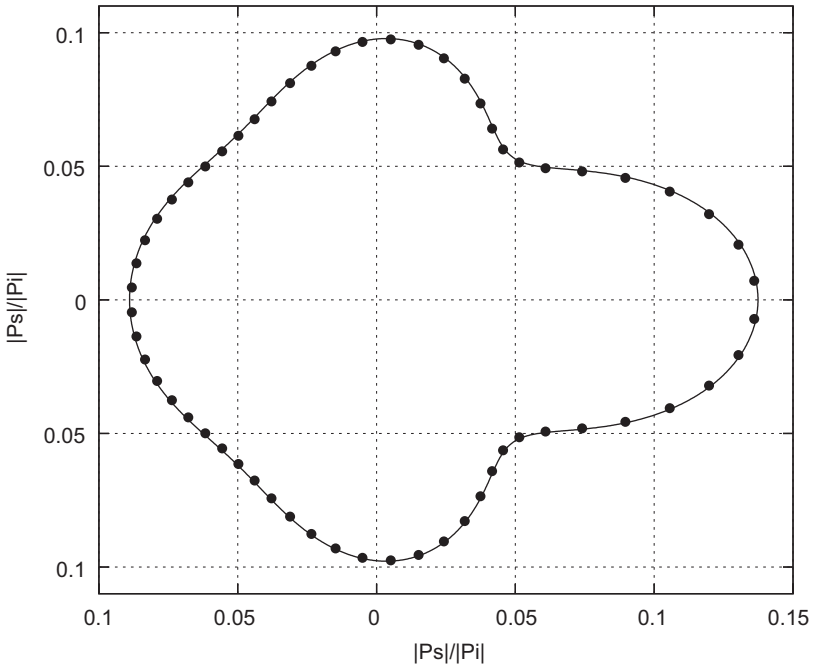

Fig. 2. Angular dependence of scattering for a plane wave impinging on a stationary sphere. $kR = 2$ and $d/R = 5$. —, analytical solution; •, numerical solution (the incident wave moves from left to right).

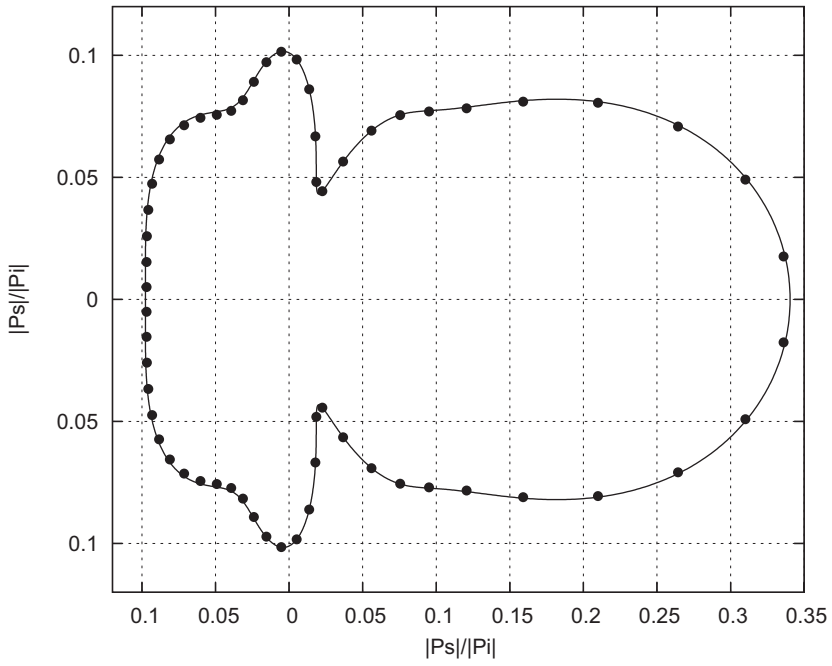

Fig. 3. Angular dependence of scattering for a plane wave impinging on a stationary sphere. $kR = 4$ and $d/R = 5$. —, analytical solution; •, numerical solution (the incident wave moves from left to right).

numerical result may be assumed to be the converged one, and perfectly matches the analytical solution. However, the prediction appears to be quite accurate even for a coarse discretization (for instance, for $N_m = N_p = 16$ the numerical solution is fairly close to the analytical one). Further comparisons between

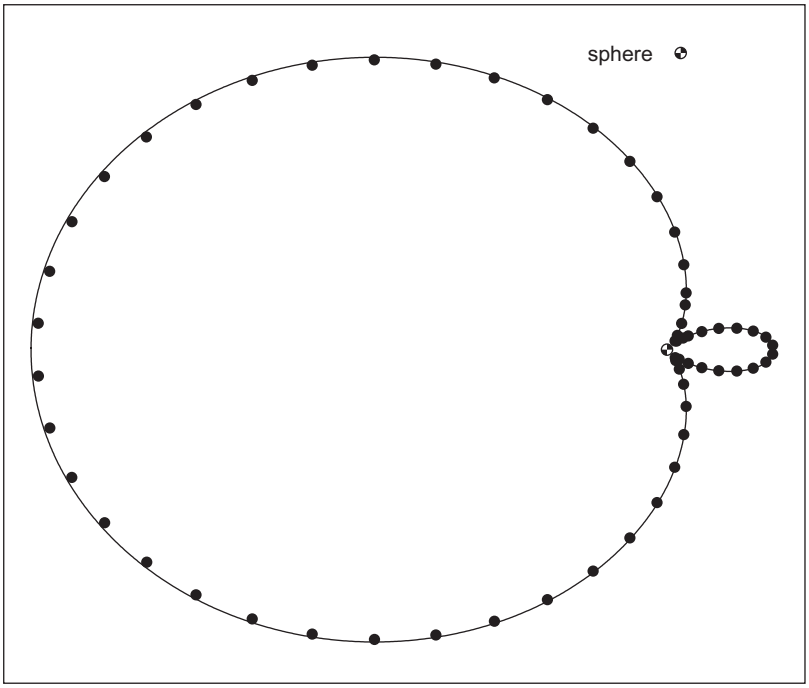

Fig. 4. Directivity patterns of scattered pressure intensity for a plane wave impinging on a stationary sphere. Far-field solution for $kR = 1$. —, analytical solution; •, numerical solution (the incident wave moves from left to right).

analytical solutions and converged numerical ones are given in Figs. 2 and 3, respectively, for $kR = 2$ and $kR = 4$. In both cases the observers are placed at a distance $d/R = 5$, and the agreement between the two solutions is excellent. The numerical results also show a similar level of accuracy in predicting the far-field scattered pressure. This is demonstrated in Figs. 4–6 where, respectively, for $kR = 1$, $kR = 2$ and $kR = 4$, the directivity patterns of the intensity of scattered pressure predicted by the formulation presented here are compared with those obtained analytically [32].

5.1.1. Elimination of spurious frequencies

A drawback in using a boundary integral method in this type of analysis arises from the so-called 'fictitious eigenvalues'. These are non-physical resonances appearing in the numerical method that can completely destroy the integral operator [3,4]. Spurious frequencies also appear in the formulation applied in this paper and correspond to the frequencies at which the matrix to be inverted in the numerical solution of the integral equation becomes singular [see Eqs. (11) and (12)]. In order to overcome this problem, here the CHIEF regularization technique introduced in Ref. [9] has been applied. This technique consists of augmenting the set of equations of the discrete form of the boundary-integral operator with homogeneous-condition equations at some points within the volume bounded by the scattering surface, followed by the application of a least-square technique for the computation of unknowns. For a stationary spherical scattering surface, the first fictitious eigenvalue appears at $kR = \pi$. For this wave number, at $d/R = 5$, Fig. 7 shows the comparison between the analytical solution, the non-regularized numerical one and the numerical one obtained through application of the regularization technique. This result demonstrates that also for the formulation proposed here, the effects of the spurious frequencies can be efficiently eliminated by application of the CHIEF approach.

5.1.2. Acoustically small spheres

Next, we examine the sound scattered by an acoustically small sphere. This case is characterized by the condition $kR \ll 1$ or, in other words, by an impinging wave length much longer than the sphere radius. The analytical solution of the scattered field is given in Ref. [33, p. 427, Eq. (9-1.8)] and has been used in Refs. [17,18] to discuss the applicability of the FW-H equation in scattering problems. In Ref. [17] it is shown

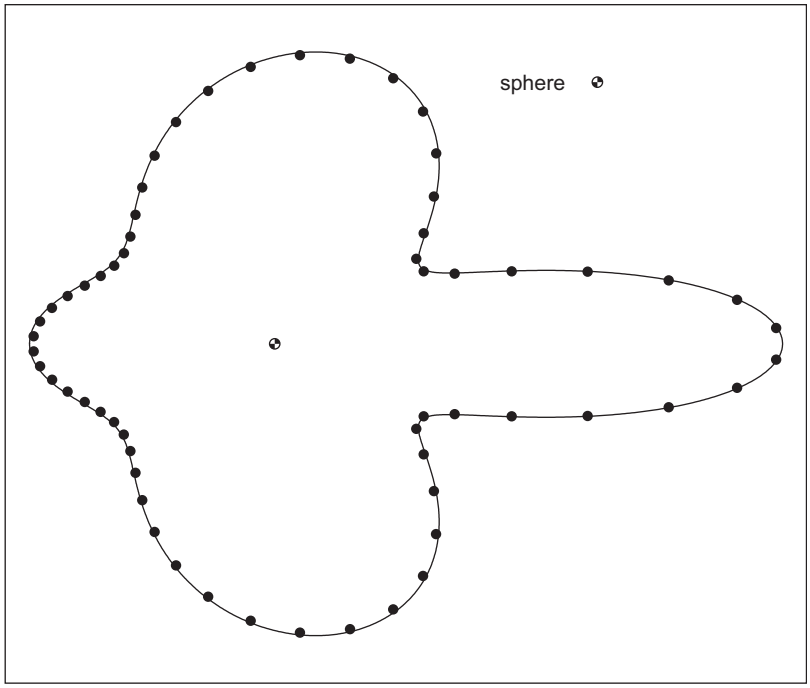

Fig. 5. Directivity patterns of scattered pressure intensity for a plane wave impinging on a stationary sphere. Far-field solution for $kR = 2$. —, analytical solution; •, numerical solution (the incident wave moves from left to right).

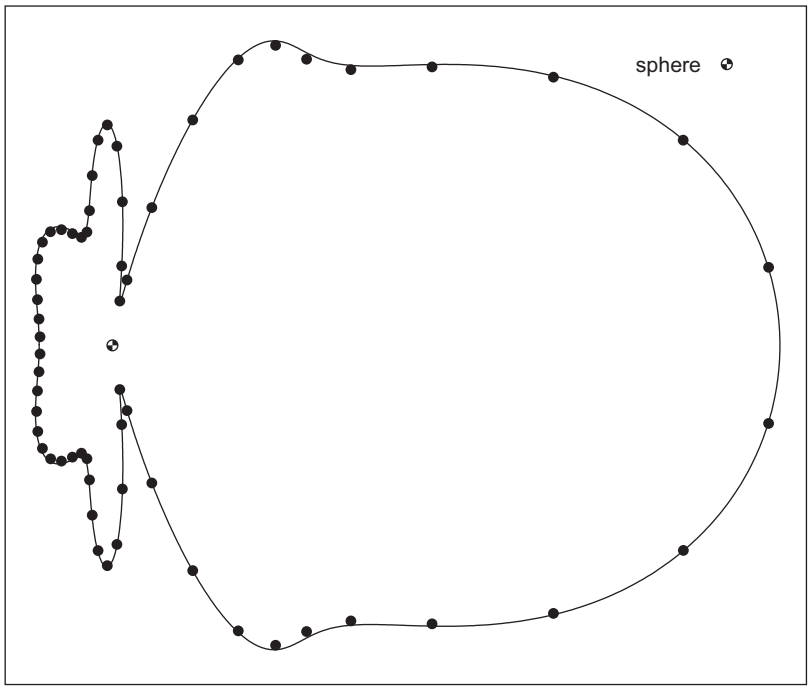

Fig. 6. Directivity patterns of scattered pressure intensity for a plane wave impinging on a stationary sphere. Far-field solution for $kR = 4$. —, analytical solution; •, numerical solution (the incident wave moves from left to right).

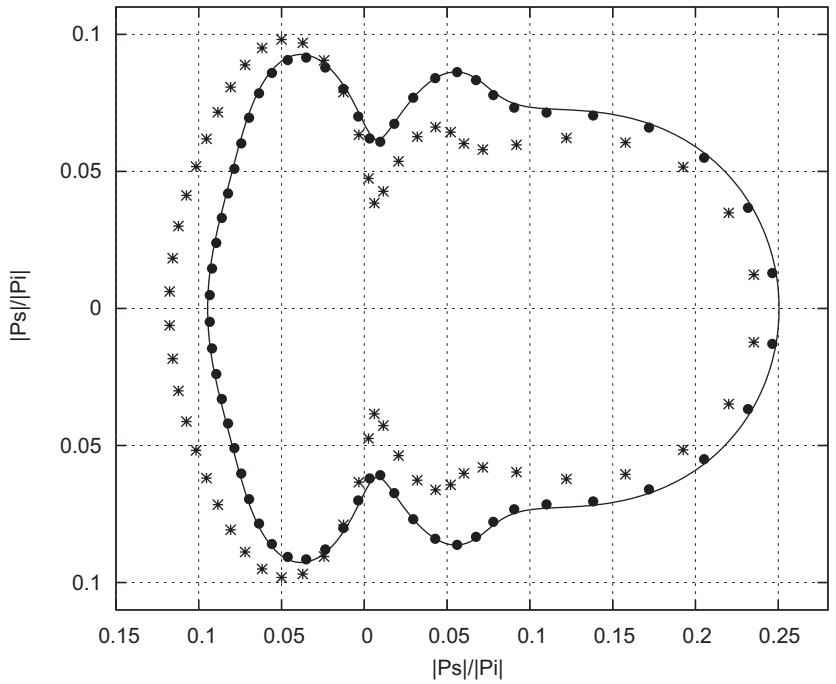

Fig. 7. Angular dependence of scattering for a plane wave impinging on a stationary sphere at the first spurious frequency. Non-regularized and regularized numerical predictions compared with the analytical solution for $kR = \pi$ and $d/R = 5$. —, analytical solution; ∗, numerical solution without CHIEF regularization; •, numerical solution with CHIEF regularization (the incident wave moves from left to right).

that the far-field solution given by a boundary integral formulation based on the FW-H equation coincides with the analytical one. This is confirmed by Fig. 8 where, for $kR = 0.15$ and $d/R = 300$, the solution obtained through the approach presented here is in excellent agreement with the analytical one. Fig. 9 depicts the comparison between the solution from the present approach and the analytical one for $kR = 0.015$ and $d/R = 1.4$. In contrast to what is claimed in Refs. [15,18], the near-field prediction from the FW-H equation perfectly matches the analytical solution. However, it is apparent that the solution obtained in Ref. [18] from the Curle equation is incorrect. Indeed, it would predict a non-zero scattered field even at $k = 0$, while it is easy to show that in this case the Curle equation reduces to a distribution of stationary, uniform dipoles and that the signal emitted by such a distribution is equal to zero.

5.2. Plane wave scattered by a stationary elastic sphere

When a pressure wave impinges a thin elastic shell, the corresponding acoustic disturbance field is the result of an aeroelastic phenomenon where incident and scattered pressure produce wall vibrations that, in turn, modify the scattered pressure field. Here, this closed-loop aeroelastic mechanism is analyzed for a plane wave impinging a spherical shell by coupling the sphere structural dynamics equations with the acoustics equations.

The discrete form of the equations of the shell structural dynamics is obtained by a modal approach. It is based on the description of elastic deformations in terms of linear combinations of modes of vibration, as given in Ref. [34]. For q denoting the vector of the corresponding Lagrangean variables, this procedure yields the following form of the dynamics equations in the frequency domain:

$$[-k^2\mathsf{M}_s + \mathsf{K}_s]\tilde{\mathsf{q}} = \tilde{\mathsf{f}}, \tag{13}$$

where M_s and K_s are, respectively, mass and stiffness matrices which depend on the geometrical (thickness, radius) and material (mass distribution, Young's modulus) properties of the shell, while f is the vector of the generalized loads that force the elastic degrees of freedom (projection of pressure onto the modes of vibration).

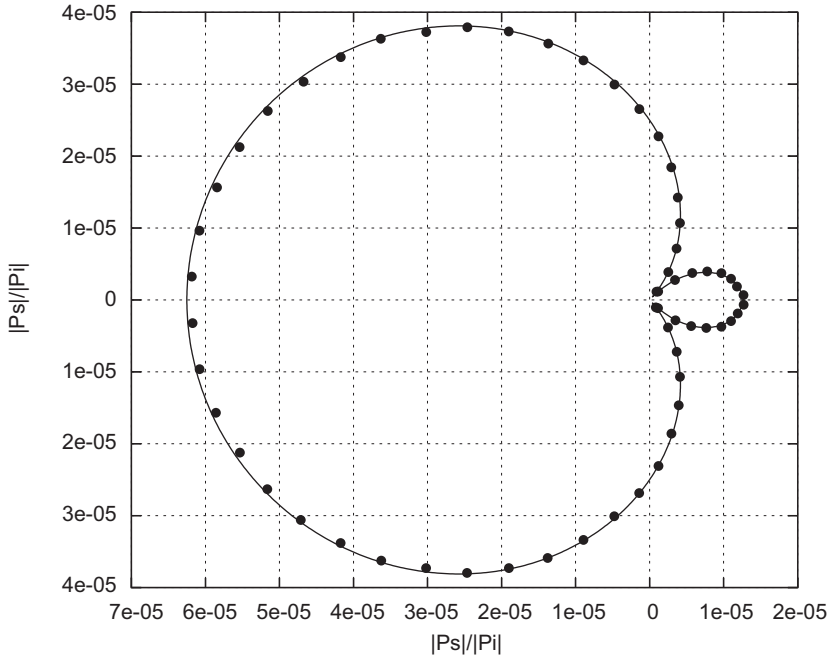

Fig. 8. Angular dependence of scattering for a plane wave impinging on a stationary acoustically small sphere. $kR = 0.15$ and $d/R = 300$. —, analytical solution; •, numerical solution (the incident wave moves from left to right).

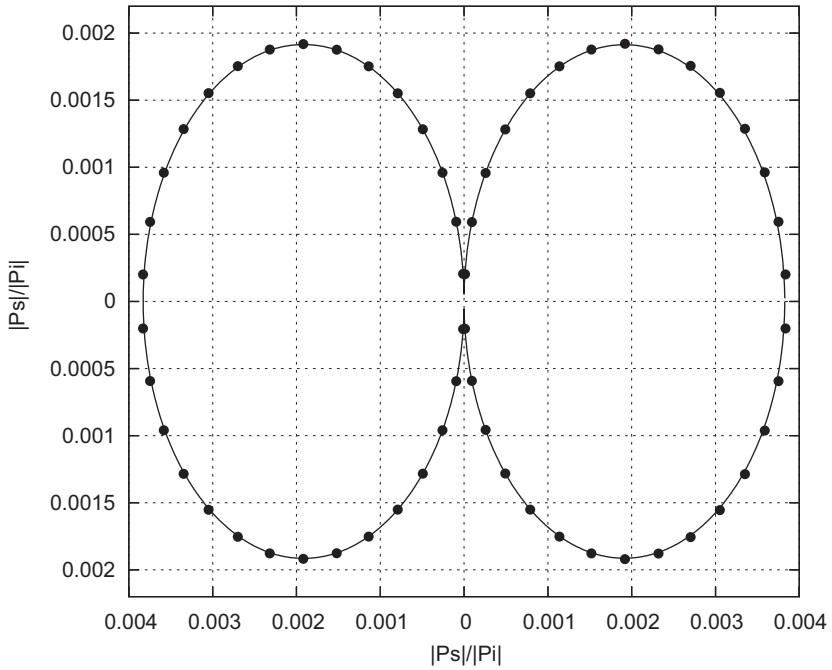

Fig. 9. Angular dependence of scattering for a plane wave impinging on a stationary acoustically small sphere. $kR = 0.015$ and $d/R = 1.4$. —, analytical solution; •, numerical solution (the incident wave moves from left to right).

From the knowledge of the modes used in the discretization of the structural dynamics equations, it is possible to relate the elastic deformation velocity to the shell Lagrangean variables through the expression $\tilde{\mathbf{x}} = \mathsf{E}_d(k)\tilde{\mathbf{q}}$, where the deformation matrix, E_d, depends on the vibration frequency and the shape of modes. Using this

deformation matrix in Eq. (10), the acoustic formulation yields

$$\tilde{\mathsf{p}}_S = \mathsf{E}_I(k)\tilde{\mathsf{p}}_I + \mathsf{E}_q(k)\tilde{\mathsf{q}}, \tag{14}$$

where $\mathsf{E}_q = \mathsf{E}_\chi \mathsf{E}_d$ is the matrix that takes into account the influence of wall vibrations on the scattered pressure over the surface. Then, defining the (projection) matrix, E_p, relating the shell surface pressure to the corresponding generalized forces [i.e., such that $\tilde{\mathsf{f}} = \mathsf{E}_p(\tilde{\mathsf{p}}_S + \tilde{\mathsf{p}}_I)$], the following acoustoelastic operator is obtained by coupling Eq. (14) with Eq. (13):

$$\tilde{\mathsf{q}} = [-k^2\mathsf{M}_s + \mathsf{K}_s - \mathsf{E}_p\mathsf{E}_q(k)]^{-1}[\mathsf{E}_p + \mathsf{E}_p\mathsf{E}_I(k)]\tilde{\mathsf{p}}_I. \tag{15}$$

Eq. (15) yields the shell elastic deformation from the knowledge of the impinging pressure, and takes into account both its direct action (through the matrix E_p) and also its indirect effects from the scattered pressure (through the matrix $\mathsf{E}_p\mathsf{E}_I$). Once the Lagrangean variables of the elastic deformation are known from Eq. (15), the scattered pressure over the shell surface is obtained by Eq. (14) and then, the scattered pressure radiated in the field is obtained through the discretized version of the integral representation in Eq. (8). Note that the acoustoelastic procedure outlined above has a general validity, in that it may be applied to elastic scatterers of arbitrary material and shape. Scatterers having different material and geometrical properties yield different mass and stiffness matrices in Eq. (13), with the corresponding shape of modes affecting both matrix E_d and matrix E_p.

For an aluminum spherical shell having thickness $T = (3/1000)R$, Fig. 10 depicts the distribution of the amplitude of the radial elastic displacement, w, along a meridian circle induced by a unit impinging plane wave with wave number $kR = 11.16$ that coincides with the first natural frequency of vibration of the structure (note that the impinging wave travels along the sphere polar axis and, therefore, the solution is constant along parallel circles). Fig. 10 presents three numerical results obtained using 30 modes for the description of the radial displacement: one is related to a surface discretization with $N_m = N_p = 40$, one is related to a surface discretization with $N_m = 40$ and $N_p = 72$, whereas the third one is the result provided by an extrapolation procedure applied to the numerical predictions obtained using different grids. The result from the finer grid is

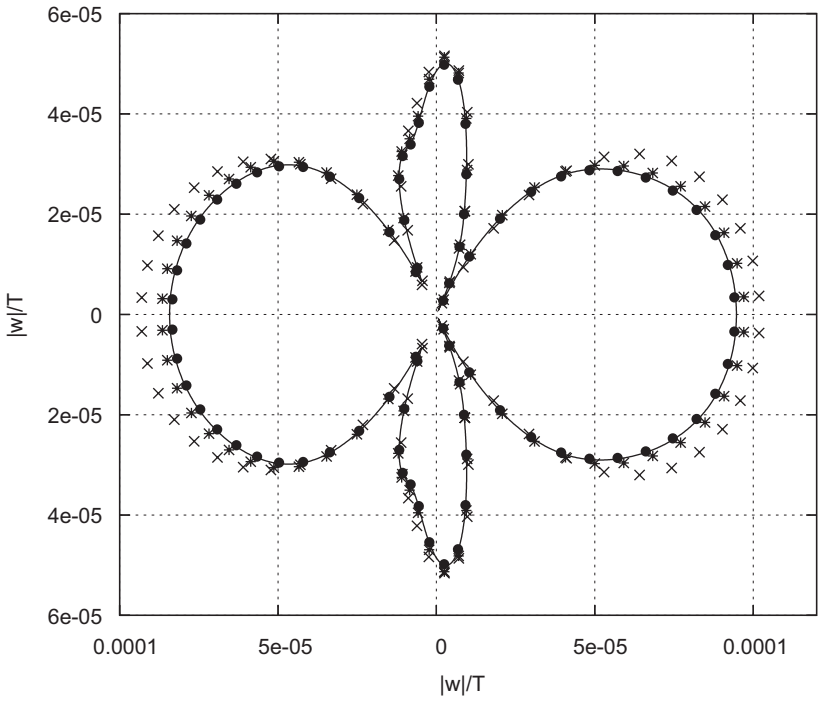

Fig. 10. Angular dependence of radial elastic displacement on the meridian circle of a sphere impinged by a plane wave with $kR = 11.16$. —, analytical solution; ×, $N_m = 40$, $N_p = 40$; ✻, $N_m = 40$, $N_p = 72$; •, extrapolated numerical solution (the incident wave moves from left to right).

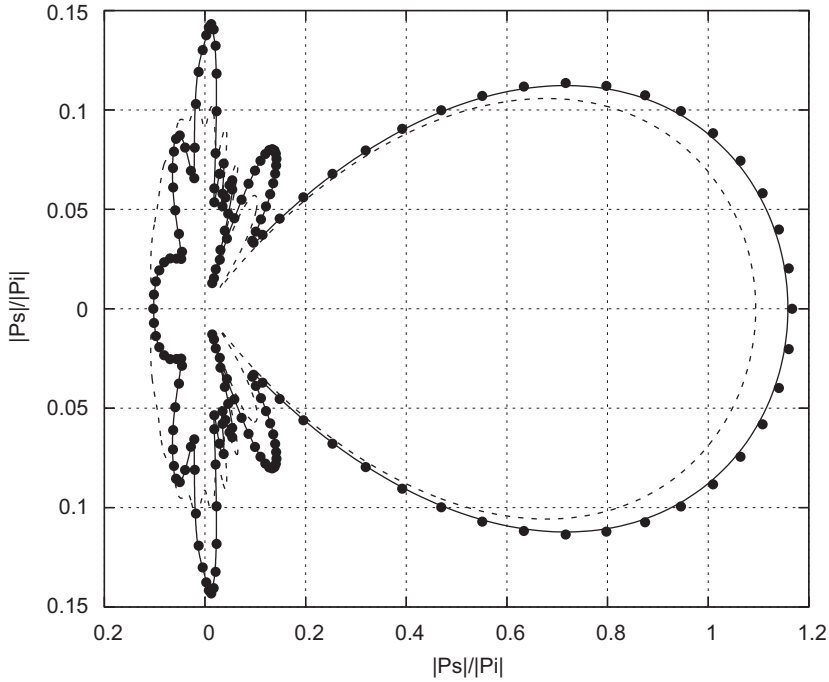

Fig. 11. Angular dependence of scattering for a plane wave impinging on a stationary elastic sphere. $kR = 11.16$ and $d/R = 5$. —, analytical solution; •, numerical solution; - - -, analytical solution (rigid sphere) (the incident wave moves from left to right).

in good agreement with the analytical solution derived following the approach presented in Ref. [35], while the extrapolated result perfectly matches it. The angular dependence of the scattered acoustic disturbance that corresponds to the elastic deformation in Fig. 10 is shown in Fig. 11. It is evaluated at a distance $d/R = 5$, where the present numerical prediction using $N_m = 40$ and $N_p = 72$ is in very good agreement with the analytical solution obtained from Ref. [35]. This figure also demonstrates that the acoustic scattering of the elastic sphere significantly differs from that produced by the undeformable body. Next, Fig. 12 depicts the pressure scattered at $d/R = 5$ by the elastic shell impinged by the plane wave with wave number $kR = 13.214$ that corresponds to the second natural frequency of vibration of the shell. Also in this case the numerical prediction obtained using $N_m = 40$ and $N_p = 72$ is in very good agreement with the analytical solution.

5.3. Scattering and vibrating moving bodies

In the following, the effect of motion on the pressure perturbation field generated by scattering and vibrating surfaces is examined.

First, consider the rigid wing scattering problem analyzed in Ref. [7]. It consists of a rectangular wing in uniform rectilinear translation at zero angle of attack, with the incident pressure field generated by a co-moving harmonic potential point source, located in its mid-span plane. The span of the wing is three times the chord length, c_w, while the cross sections have a symmetric biconvex parabolic shape with thickness ratio $t_w/c_w = 0.1$. For $(\mathbf{x}_0, x, y, z)$ denoting a wing-fixed coordinate system having chordwise x-axis, spanwise y-axis and origin, $\mathbf{x}_0$, at the center of the mid-span cross section (see Fig. 13), Figs. 14 and 15 depict directivity patterns of pressure scattered in the mid-span plane at radial distance $d/c_w = 52.5$ from $\mathbf{x}_0$ by the wing moving in the negative x-axis direction at velocity $\mathbf{v}$ corresponding to Mach number $M = 0.5$ (see Fig. 13). Specifically, for wave number $kc_w = 6$, the results in Fig. 14 concern the source point located above the leading edge at $\mathbf{x}_s^{\mathrm{LE}} = (-5c_w, 0, 5c_w)$, while those in Fig. 15 concern the source point located above the trailing edge at $\mathbf{x}_s^{\mathrm{TE}} = (5c_w, 0, 5c_w)$ (see Fig. 13). These figures compare the predictions given by the present formulation with those obtained through a linear velocity-potential approach based on the integral formulation described in Refs. [21,22], which is equivalent to that used in Ref. [7]. The results are presented in terms of the ratio

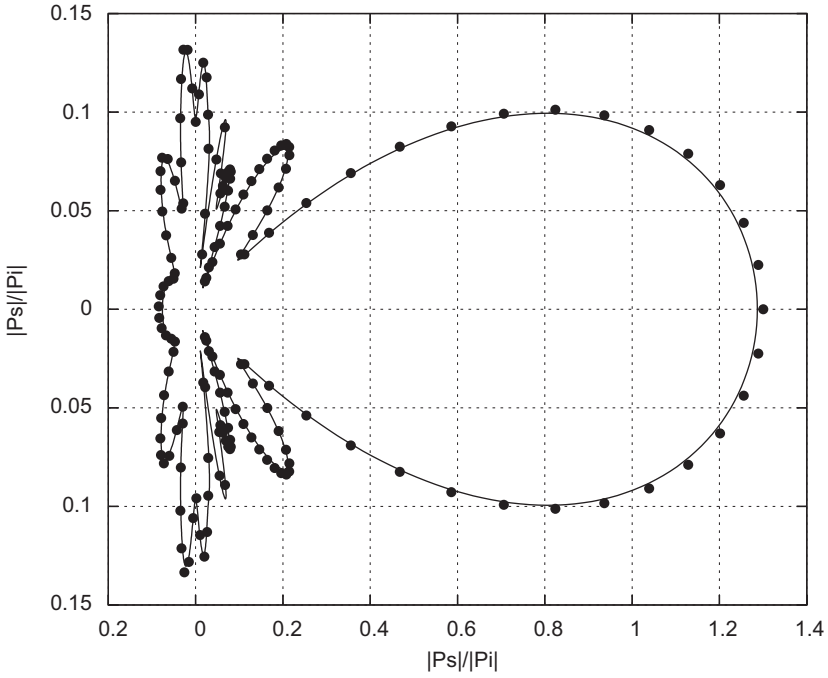

Fig. 12. Angular dependence of scattering for a plane wave impinging on a stationary elastic sphere. $kR = 13.214$ and $d/R = 5$. —, analytical solution; •, numerical solution (the incident wave moves from left to right).

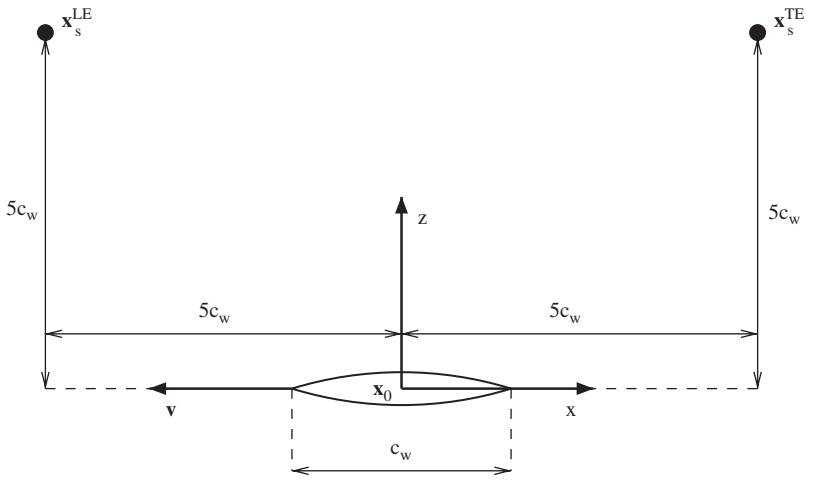

Fig. 13. Mid-plane of the scattering wing. Wing velocity and location of point sources.

between the scattered pressure and a reference pressure defined as $p_{\text{ref}} = 2d|\tilde{p}'_I(\mathbf{x}_0, k)|/c_w$ [7]. As expected, the results obtained from the potential approach are in perfect agreement with those presented in Ref. [7], but show significant discrepancies with respect to the predictions obtained through the formulation based on the FW-H equation, especially in the region closer to the source (i.e., in front of the leading edge in Fig. 14 and in front of the trailing edge in Fig. 15). This disagreement is quite unexpected and could be due to the different effect that the elimination of the nonlinear terms has on the two solutions. In the present approach, when subsonic configurations are examined, the quadrupole term disappears in sound radiation (observer far from the body), but might become relevant when the integral formulation is used as an integral equation

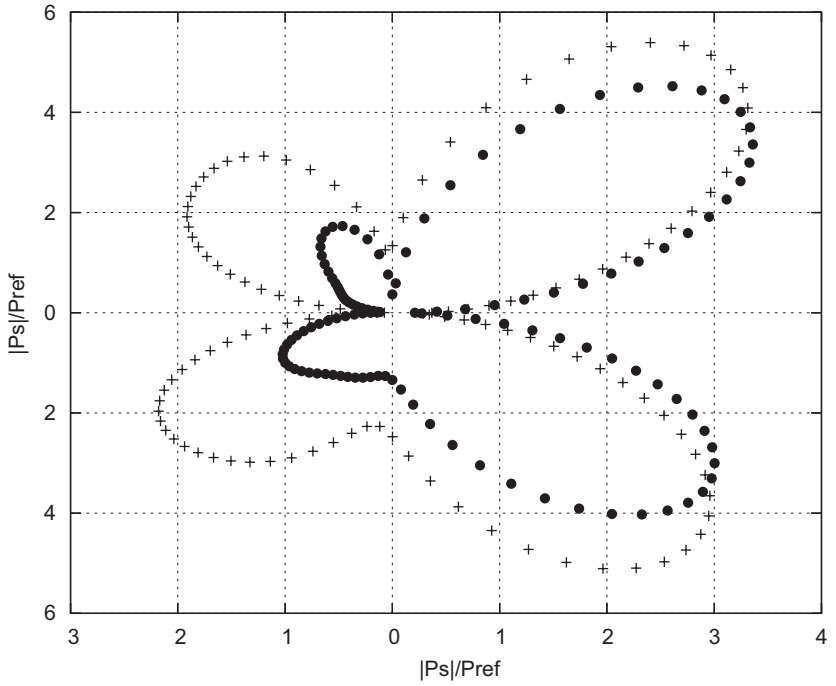

Fig. 14. Pressure scattered in mid-span plane by a wing in uniform rectilinear translation. Source point at $\mathbf{x}_s^{\mathrm{LE}} = (-5c_w, 0, 5c_w)$, $kc_w = 6$, $d/c_w = 52.5$, $M = 0.5$. +, potential solution; •, FW-H solution (the wing moves from right to left).

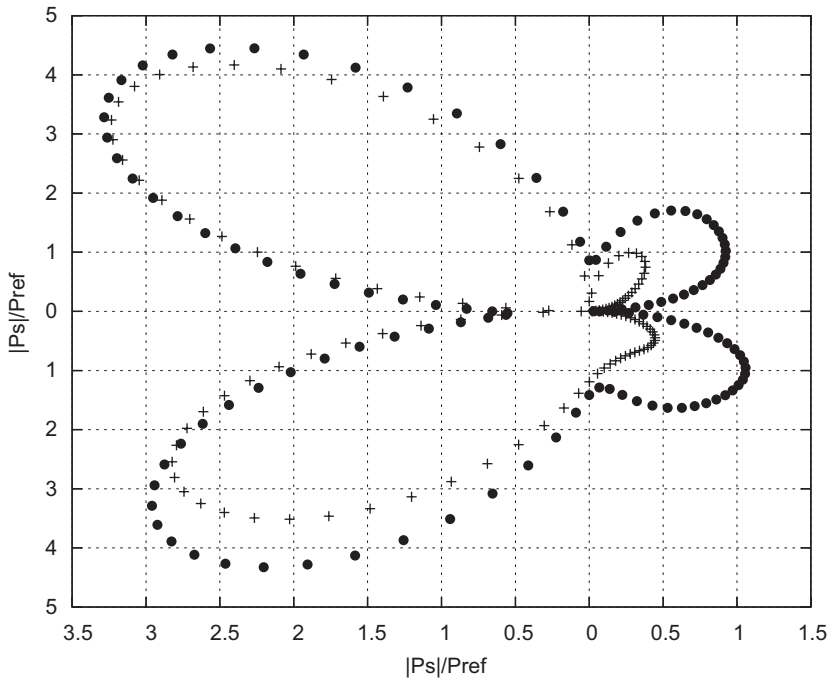

Fig. 15. Pressure scattered in mid-span plane by a wing in uniform rectilinear translation. Source point at $\mathbf{x}_s^{\mathrm{TE}} = (5c_w, 0, 5c_w)$, $kc_w = 6$, $d/c_w = 52.5$, $M = 0.5$. +, potential solution; •, FW-H solution (the wing moves from right to left).

(observer on the body), unless the Lighthill tensor is very small. Note that the perturbed Lighthill tensor would give rise to linear perturbation terms which could become important as the body Mach number increases, in that proportional to the local unperturbed flow velocity, $\mathbf{u}_0$, on the body surface. Indeed, the scattered fields predicted by potential and FW-H formulations are quite similar as the Mach number decreases to $M = 0.1$, while they become almost identical in the steady-wing case, as shown in Figs. 16 and 17, respectively (in both cases the potential point source is located at $\mathbf{x}_s^{\mathrm{LE}}$). The importance of the nonlinear terms is also analyzed in Fig. 18, which shows the steady pressure perturbation at distance $d/c_w = 5$ due to the uniform motion of the wing at $M = 0.5$. In this case, the predictions from the two formulations are in good agreement for $t_w/c_w \leqslant 0.1$, while significant discrepancies start arising for $t_w/c_w = 0.2$, particularly at observer locations in front of the wing regions where the highest values of fluid flow velocity occur and the Lighthill tensor is greater (for these results, $p_{\mathrm{ref}} = 0.5\rho_0 c^2 M^2$). Note that the pressure examined in Fig. 18 corresponds to the rigid-body motion perturbation field, p'_R, mentioned in Section 4, and these results confirm what was claimed at the beginning of the same section.

Finally, a rigid vibrating sphere is examined. It is considered in uniform rectilinear translation, while oscillating back and forth along the direction of motion, with $kR = 1$. The results from the present formulation are compared with those from a linearized velocity potential approach in terms of the ratio $|\tilde{p}'|/p_{\mathrm{ref}}$, where $p_{\mathrm{ref}} = \rho_0 cU$, with U denoting the magnitude of sphere oscillations. Figs. 19 and 20 depict the acoustic disturbance distribution on a surface meridian circle parallel to the direction of motion, respectively, for $M = 0.1$ and 0.2, in addition to that for $M = 0$. Similar to the wing scattering problem, the agreement between the two formulations is excellent for $M = 0$, but worsens as the Mach number increases, although remaining quite similar up to $M = 0.2$. The two approaches predict that, at both Mach numbers, the uniform translation induces an increase of the pressure disturbance in the front region, while in the rear part the pressure disturbance is slightly reduced at $M = 0.1$ and slightly increased at $M = 0.2$ (the sphere moves from right to left). Note that these results differ from those presented in Ref. [36] where the same problem has been analyzed using a formulation very close to that presented here. In particular, the results presented in Ref. [36] seem to overestimate the pressure perturbation in the front region and to underestimate it in the rear part.

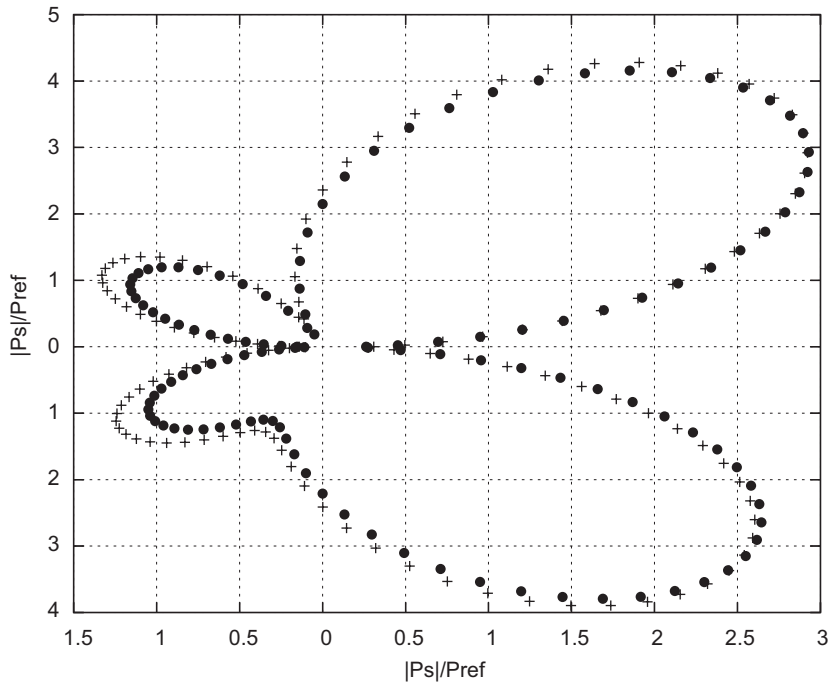

Fig. 16. Pressure scattered in mid-span plane by a wing in uniform rectilinear translation. Source point at $\mathbf{x}_s^{\mathrm{LE}} = (-5c_w, 0, 5c_w)$, $kc_w = 6$, $d/c_w = 52.5$, $M = 0.1$. +, potential solution; •, FW-H solution (the wing moves from right to left).

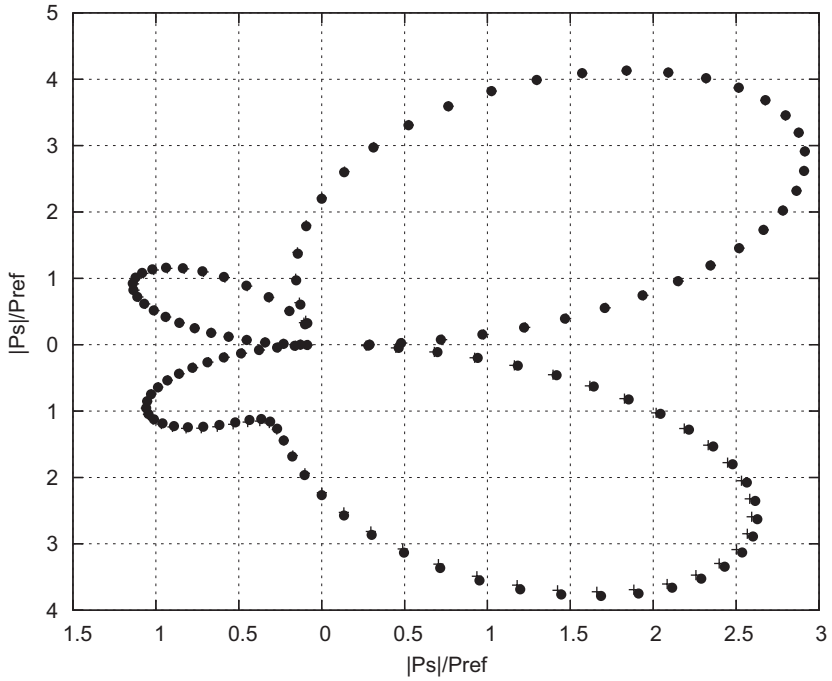

Fig. 17. Pressure scattered in mid-span plane by a stationary wing. Source point at $\mathbf{x}_s^{\mathrm{LE}} = (-5c_w, 0, 5c_w)$, $kc_w = 6$, $d/c_w = 52.5$. +, potential solution; •, FW-H solution.

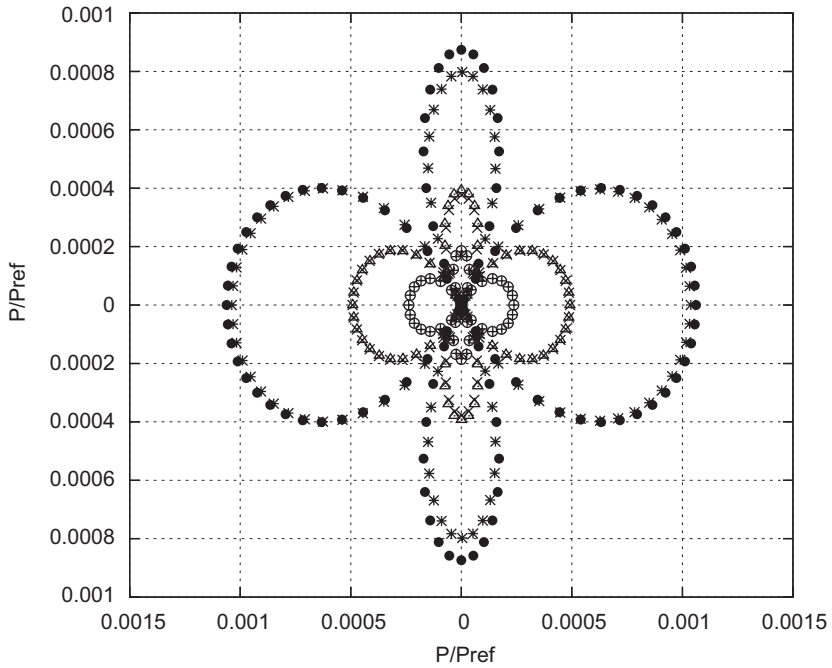

Fig. 18. Pressure steady perturbation in mid-span plane due to a wing in uniform rectilinear translation at $M = 0.5$. $d/c_w = 5$. +, potential solution, $t_w/c_w = 0.05$; ○, FW-H solution, $t_w/c_w = 0.05$; ×, potential solution, $t_w/c_w = 0.1$; △, FW-H solution, $t_w/c_w = 0.1$; ✻, potential solution, $t_w/c_w = 0.2$; •, FW-H solution, $t_w/c_w = 0.2$ (the wing moves from right to left).

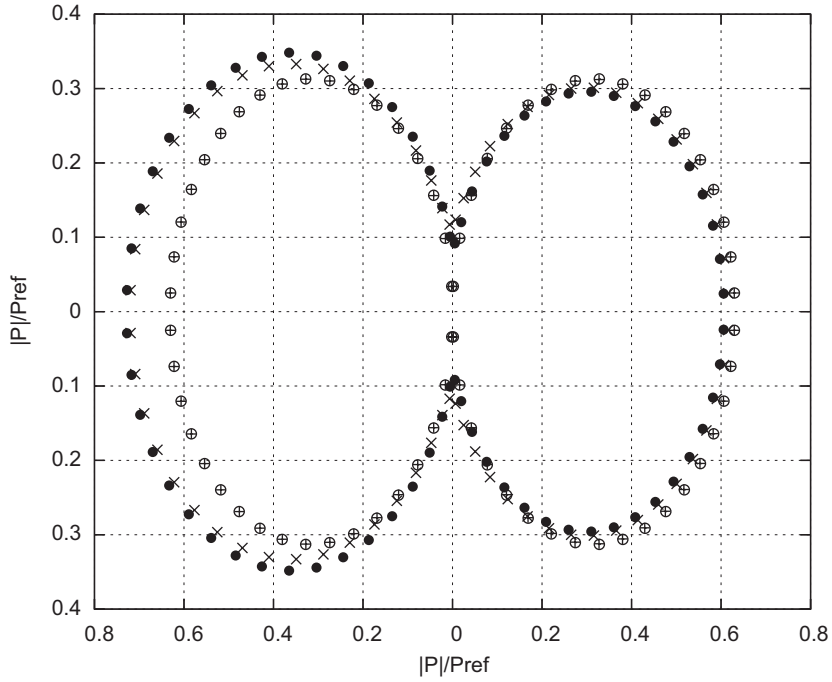

Fig. 19. Angular dependence of pressure perturbation on the surface of a rigid sphere in uniform rectilinear translation, oscillating back and forth along the direction of motion. $kR = 1$. +, potential solution, $M = 0$; ○, FW-H solution, $M = 0$; ×, potential solution, $M = 0.1$; •, FW-H solution, $M = 0.1$ (the sphere moves from right to left).

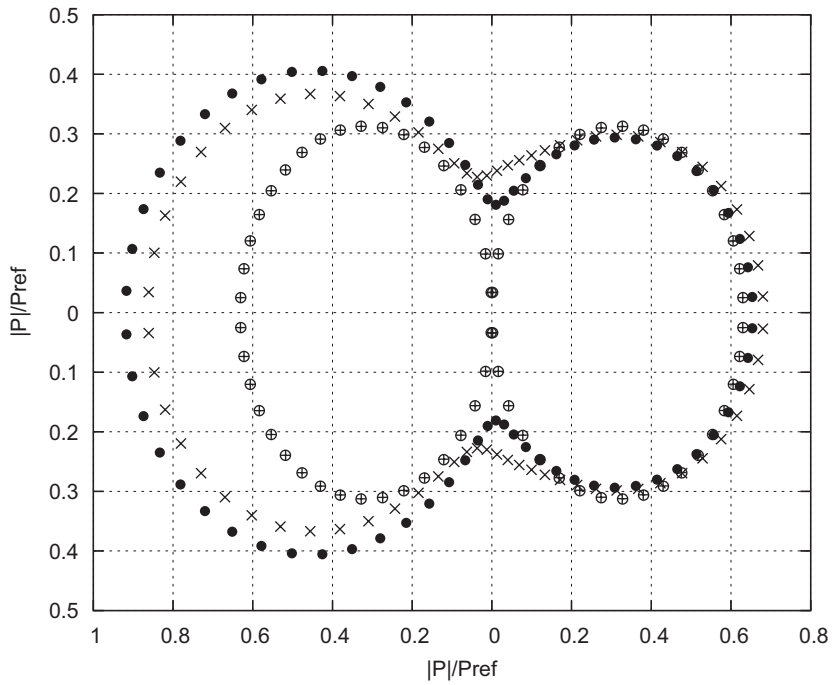

Fig. 20. Angular dependence of pressure perturbation on the surface of a rigid sphere in uniform rectilinear translation, oscillating back and forth along the direction of motion. $kR = 1$. +, potential solution, $M = 0$; ○, FW-H solution, $M = 0$; ×, potential solution, $M = 0.2$; •, FW-H solution, $M = 0.2$ (the sphere moves from right to left).

6. Conclusions

The formulation presented in this work yields a unified approach for the prediction of surface pressure perturbations and sound radiation generated by pressure waves impinging moving, elastic bodies. It can also be conveniently applied to those aeronautical configurations where one major source of noise generated by aerodynamics may be identified. Indeed, if such a source of noise may be assumed to be aerodynamically independent from the other bodies, this methodology yields the overall pressure perturbation with inclusion of interactional acoustic effects, requiring only its aerodynamic solution as an input. In particular, the scattering effects are determined from the knowledge of the impinging pressure, and this is a considerable simplification with respect to those widely used scattering formulations where the normal derivative of the incident pressure over the scatterer surface is needed. Although valid for bodies with a rigid contour, the proposed formulation includes elastic vibration as a porosity effect, and thus can be applied to vibroacoustic/acoustoelastic problems. The numerical investigation has demonstrated that it gives very accurate predictions of near- and far-field pressure scattered by stationary rigid spheres, both for low-frequency and for mid-frequency incident waves. Very accurate numerical predictions have also been obtained for scattering problems concerning stationary elastic surfaces, both in terms of the resulting elastic deformations and in terms of radiated sound. The problem of the presence of spurious frequency in the integral operator has been discussed and solved by the widely used CHIEF regularization technique. Finally, the present formulation has been applied to scattering and vibrating surfaces in uniform motion. The results have been compared with those given by a linearized velocity potential formulation showing that discrepancies grow together with the body velocity number. This might be due to the fact that the nonlinear terms that have not been included could become non negligible as the velocity increases, yielding a quantitative different influence in the two formulations. In particular, in the present approach the quadrupole term might become relevant when the observer is on the body, unless the Lighthill tensor is very small. This is an open issue which deserves further research.

Appendix A. Integral contribution from kernel singularity

When the integral equation in Eq. (5) is derived from Eq. (2) by letting the observer position, $\mathbf{x}$, approach the surface, S_B, singularities of kernel functions $\hat{G}$ and $\nabla\hat{G}$ arise. In the integrals with kernel $\hat{G}$ the singularity is removed by combination with the differential of the surface area and they are integrable in the ordinary sense. On the contrary, the integrals with kernel $\nabla\hat{G}$ are of improper singular type and their evaluation may be obtained performing the limit $\mathbf{x} \to S_B$. In the following, it will be shown that this limit is finite, yielding the regularized form of the singular integral as the sum of a so-called free term evaluated at the observer position [37] and a convergent improper integral.

Consider an integral term of the type

$$\mathfrak{I}(\mathbf{x}, t) = \int_S [\mathbf{z} \cdot \nabla\hat{G}]_{\text{ret}} \, \mathrm{d}S$$

in which, for $\mathbf{x} \to \mathbf{x}_0 \in S$, the kernel function $\nabla\hat{G}$ shows a singularity at $\mathbf{y} = \mathbf{x}_0$. The evaluation of the singular contribution may be performed in the limit $\mathbf{x} \to S$, and for this purpose it is convenient to decompose the domain of integration in the following way:

$$\begin{aligned} \mathfrak{I}(\mathbf{x}_0, t) &= \mathfrak{I}_s(\mathbf{x}_0, t) + \mathfrak{I}_r(\mathbf{x}_0, t) \\ &= \lim_{\mathbf{x}\to\mathbf{x}_0} \int_{S_\varepsilon} [\mathbf{z} \cdot \nabla\hat{G}]_{\text{ret}} \, \mathrm{d}S + \lim_{\mathbf{x}\to\mathbf{x}_0} \int_{S\setminus S_\varepsilon} [\mathbf{z} \cdot \nabla\hat{G}]_{\text{ret}} \, \mathrm{d}S, \end{aligned} \tag{16}$$

where S_ε is an arbitrarily shaped small portion of surface of characteristic length ε containing $\mathbf{x}_0$, such that its boundary tends to collapse onto it for $\varepsilon \to 0$. The second integral, $\mathfrak{I}_r$, denotes the regular contribution from the portion of surface that does not contain singularities. The evaluation of the limit of the first integral, $\mathfrak{I}_s$, is the aim of this appendix.

Let us introduce a local orthogonal coordinate system, $(\mathbf{x}_0, s, l, n)$, co-moving with the surface, with the origin at $\mathbf{x}_0$, n normal to the surface, and the plane (s, n) containing the vector, $\mathbf{v}$, of the local velocity of the

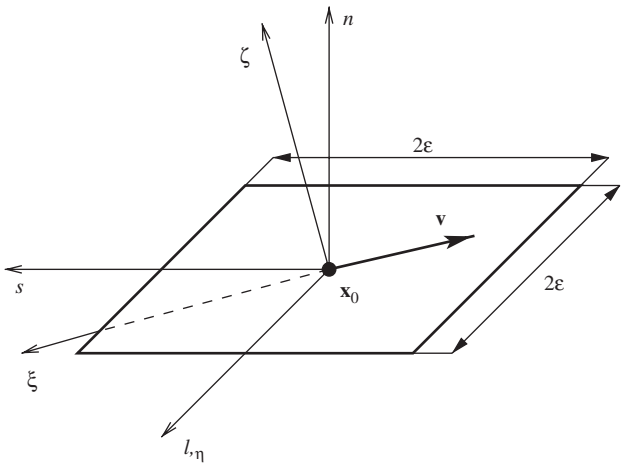

Fig. 21. Local coordinates co-moving with S_ε.

surface (see Fig. 21). Denoting with z_s, z_l, z_n the components of the vector $\mathbf{z}$ in this coordinate system, assuming that $|\mathbf{x}-\mathbf{x}_0| = a\varepsilon^\mu$ with a representing an arbitrary constant and $\mu>1$, for $\varepsilon \to 0$ the integral $\mathfrak{I}_s$ becomes

$$\mathfrak{I}_s(\mathbf{x}_0,t) = z_s(\mathbf{x}_0,t)\lim_{\varepsilon\to 0}\int_{S_\varepsilon}\frac{\partial \hat{G}}{\partial s}\,\mathrm{d}S + z_l(\mathbf{x}_0,t)\lim_{\varepsilon\to 0}\int_{S_\varepsilon}\frac{\partial \hat{G}}{\partial l}\,\mathrm{d}S + z_n(\mathbf{x}_0,t)\lim_{\varepsilon\to 0}\int_{S_\varepsilon}\frac{\partial \hat{G}}{\partial n}\,\mathrm{d}S$$

in that

$$\lim_{\varepsilon\to 0}\int_{S_\varepsilon}[[\mathbf{z}(\mathbf{y},\tau)-\mathbf{z}(\mathbf{x}_0,t)]\cdot\nabla\hat{G}]_{\mathrm{ret}}\,\mathrm{d}S = 0$$

under the hypothesis that the function $\mathbf{z}\in C^{0,\alpha}(S_\varepsilon)$, i.e., is a bounded uniformly Hölder continuous function for $\mathbf{y}\in S_\varepsilon$, with exponent $0<\alpha\leqslant 1$ [37,38].

Next, rewriting the normal derivative of $\hat{G}$ as

$$\frac{\partial \hat{G}}{\partial n} = \frac{\partial \hat{G}}{\partial n} - \mathbf{M}\cdot\mathbf{n}\mathbf{M}\cdot\nabla\hat{G} + \mathbf{M}\cdot\mathbf{n}\mathbf{M}\cdot\nabla\hat{G} = \frac{\partial \hat{G}}{\partial \check{n}} + M_n^2\frac{\partial \hat{G}}{\partial n} + M_n M_s\frac{\partial \hat{G}}{\partial s}$$

with $\mathbf{M} = \mathbf{v}(\mathbf{x}_0,t)/c$, $M_n = v_n(\mathbf{x}_0,t)/c$, $M_s = v_s(\mathbf{x}_0,t)/c$ and $\partial(\ldots)/\partial\check{n} = \partial(\ldots)/\partial n - \mathbf{M}\cdot\mathbf{n}\mathbf{M}\cdot\nabla(\ldots)$, yields the following expression for the singular integral:

$$\begin{aligned}\mathfrak{I}_s(\mathbf{x}_0,t) = {} & [z_s(\mathbf{x}_0,t) + z_n(\mathbf{x}_0,t)M_nM_s/\beta_n^2]\lim_{\varepsilon\to 0}\int_{S_\varepsilon}\frac{\partial \hat{G}}{\partial s}\,\mathrm{d}S \\ & + z_l(\mathbf{x}_0,t)\lim_{\varepsilon\to 0}\int_{S_\varepsilon}\frac{\partial \hat{G}}{\partial l}\,\mathrm{d}S + [z_n(\mathbf{x}_0,t)/\beta_n^2]\lim_{\varepsilon\to 0}\int_{S_\varepsilon}\frac{\partial \hat{G}}{\partial \check{n}}\,\mathrm{d}S,\end{aligned} \tag{17}$$

where $\beta_n^2 = 1 - M_n^2$.

In Eq. (17) the first two integrals disappear, for $\varepsilon \to 0$, if S_ε is symmetric with respect to $\mathbf{x}_0$. To show this, let us choose, arbitrarily but legitimately, S_ε as a square with edge length equal to 2ε and also introduce a local coordinate system, $(\mathbf{x}_0,\xi,\eta,\zeta)$, co-moving with the surface. The origin of the coordinate system is located at the center of S_ε, the ξ-axis is aligned with the local surface velocity, $\mathbf{v}$ [and thus lies in the plane (s,n)], while the η-axis coincides with the l-axis (see Fig. 21). For $\varepsilon \to 0$ the source–observer time delay tends to zero and in the present analysis it is possible to approximate the motion of S_ε as a uniform translation with velocity equal to that of $\mathbf{x}_0$ at the observer time. In this case, observing that for a source in uniform translation at a

given time, t, one has [22,32]

$$\hat{G}(\mathbf{x},\boldsymbol{\eta}) = \frac{1}{4\pi}\left[\frac{-1}{r(1-M_r)}\right]_{\text{ret}} = \frac{-1}{4\pi r_\beta},$$

where $r_\beta(\mathbf{x},\boldsymbol{\eta}) = \sqrt{[\xi(\mathbf{x})-\xi]^2 + \beta^2\{[\eta(\mathbf{x})-\eta]^2 + [\zeta(\mathbf{x})-\zeta]^2\}}$, with $\beta = \sqrt{1-M^2}$, it is easy to recognize that, for $\mathrm{d}S = \mathrm{d}s\,\mathrm{d}l$

$$\lim_{\varepsilon\to 0}\int_{S_\varepsilon}\frac{\partial\hat{G}}{\partial l}\,\mathrm{d}S = \lim_{\varepsilon\to 0}\int_{-\varepsilon}^{\varepsilon}[\hat{G}(\mathbf{x},\boldsymbol{\eta}(s,\varepsilon)) - \hat{G}(\mathbf{x},\boldsymbol{\eta}(s,-\varepsilon))]\,\mathrm{d}s = 0 \tag{18}$$

and

$$\lim_{\varepsilon\to 0}\int_{S_\varepsilon}\frac{\partial\hat{G}}{\partial s}\,\mathrm{d}S = \lim_{\varepsilon\to 0}\int_{-\varepsilon}^{\varepsilon}[\hat{G}(\mathbf{x},\boldsymbol{\eta}(\varepsilon,l)) - \hat{G}(\mathbf{x},\boldsymbol{\eta}(-\varepsilon,l))]\,\mathrm{d}l = 0. \tag{19}$$

Indeed, $r_\beta(\mathbf{x}_0,\boldsymbol{\eta}) = \sqrt{\xi^2+\beta^2[\eta^2+\zeta^2]}$; thus, $\hat{G}(\mathbf{x}_0,\boldsymbol{\eta}(s,l)) = \hat{G}(\mathbf{x}_0,\boldsymbol{\eta}(s,-l))$ and $\hat{G}(\mathbf{x}_0,\boldsymbol{\eta}(s,l)) = \hat{G}(\mathbf{x}_0,\boldsymbol{\eta}(-s,l))$ for any $s\in[-\varepsilon,\varepsilon]$, $l\in[-\varepsilon,\varepsilon]$ (see Fig. 21).

Finally, for the evaluation of the third integral in Eq. (17) the Prandtl–Glauert transformation of coordinates

$$\hat{\xi} = \xi/\beta, \quad \hat{\eta} = \eta, \quad \hat{\zeta} = \zeta$$

is conveniently applied. Noting that the Prandtl–Glauert space coordinates yield

$$r_\beta(\mathbf{x},\boldsymbol{\eta}) = \beta\hat{r}(\mathbf{x},\boldsymbol{\eta}),$$

where

$$\hat{r}(\mathbf{x},\boldsymbol{\eta}) = \sqrt{[\hat{\xi}(\mathbf{x})-\hat{\xi}(\boldsymbol{\eta})]^2 + [\hat{\eta}(\mathbf{x})-\hat{\eta}(\boldsymbol{\eta})]^2 + [\hat{\zeta}(\mathbf{x})-\hat{\zeta}(\boldsymbol{\eta})]^2}$$

is the source–observer distance in the Prandtl–Glauert space, it is possible to show that the third integral in Eq. (17) may be recast in the following way (see Ref. [22]):

$$\int_{S_\varepsilon}\frac{\partial\hat{G}}{\partial\check{n}}\,\mathrm{d}S = \frac{1}{4\pi}\int_{\hat{S}_\varepsilon}\frac{\partial}{\partial\hat{n}}\left(\frac{-1}{\hat{r}}\right)\mathrm{d}\hat{S} \tag{20}$$

with $\hat{S}_\varepsilon$ and $\partial(\ldots)/\partial\hat{n}$ denoting the image of S_ε and the normal derivative in the Prandtl–Glauert space, respectively. The integral on the right-hand side of the equation above coincides with a double-layer potential with unit density. For our purposes, it may conveniently be interpreted in terms of solid angles. Indeed, with the normal derivative performed with respect to the source space variable, note that

$$\frac{\partial}{\partial\hat{n}}\left(\frac{-1}{\hat{r}}\right)\mathrm{d}\hat{S} = -\frac{\hat{\mathbf{n}}\cdot\hat{\mathbf{r}}}{\hat{r}^3}\,\mathrm{d}\hat{S} = -\mathrm{sgn}(\hat{\mathbf{n}}\cdot\hat{\mathbf{r}})\frac{1}{\hat{r}^2}\cos\alpha\,\mathrm{d}\hat{S} = -\mathrm{sgn}(\hat{\mathbf{n}}\cdot\hat{\mathbf{r}})\,\mathrm{d}\Omega,$$

where α is the angle between the normal direction and the source–observer direction in the Prandtl–Glauert space, $\mathrm{sgn}(\hat{\mathbf{n}}\cdot\hat{\mathbf{r}})$ denotes the sign of the scalar product between $\hat{\mathbf{r}}$ and $\hat{\mathbf{n}}$, while $\mathrm{d}\Omega = \mathrm{d}\hat{S}\cos\alpha/\hat{r}^2$ is the solid angle element, i.e., the surface element that $\mathrm{d}\hat{S}$ projects upon the unit sphere centered at the point $\hat{\mathbf{x}}$ that denotes the image of the observer point in the Prandtl–Glauert space (see Fig. 22, where $\hat{\mathbf{x}}_0$ represents the image of $\mathbf{x}_0$ in the Prandtl–Glauert space). Hence, the integration of a double-layer potential with unit density over a closed surface is equal to zero for $\mathbf{x}$ outside it, whereas it is equal to one for $\mathbf{x}$ inside it (and outward unit normal vector). In our case, for $\mathbf{x}$ approaching $\mathbf{x}_0$ from outside (i.e., for $\hat{\mathbf{n}}\cdot\hat{\mathbf{r}}>0$), and assuming a regular surface in its neighborhood, one has

$$\lim_{\varepsilon\to 0}\frac{1}{4\pi}\int_{\hat{S}_\varepsilon}\frac{\partial}{\partial\hat{n}}\left(\frac{-1}{\hat{r}}\right)\mathrm{d}\hat{S} = -\frac{1}{2} \tag{21}$$

in that, for $\varepsilon\to 0$, the solid angle through which $\hat{S}_\varepsilon$ is seen by the observer is equal to 2π. Note that this result is not dependent on the shape of the surface S_ε considered, as expected from the integration of a weakly singular kernel like the double-layer potential [38] (the same result may also be obtained using a mathematical

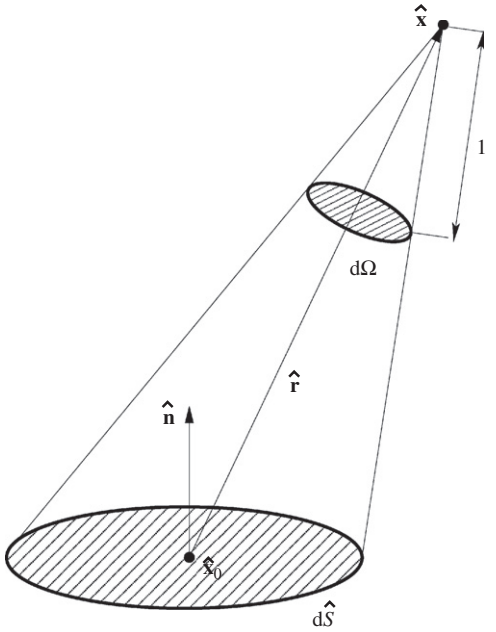

Fig. 22. Solid angle through which $d\hat{S}$ is seen by an observer at $\hat{\mathbf{x}}$.

rather than a geometrical approach, as shown in Ref. [39]). Combining Eqs. (17)–(21) yields

$$\mathfrak{I}_s(\mathbf{x}_0, t) = -\frac{z_n(\mathbf{x}_0, t)}{2\beta_n^2}$$

that, recalling Eq. (16), provides the following final expression for the singular integral examined:

$$\mathfrak{I}(\mathbf{x}_0, t) = -\frac{z_n(\mathbf{x}_0, t)}{2\beta_n^2} + \lim_{\varepsilon \to 0} \int_{S \setminus S_\varepsilon} [\mathbf{z} \cdot \nabla \hat{G}]_{\text{ret}} \, dS, \tag{22}$$

where the first term is the free term contribution to the integral emerging from the singularity arising as $\mathbf{x} \to \mathbf{x}_0$. In order to interpret the second integral term it is convenient to recast the integrand $\mathbf{z} \cdot \nabla \hat{G}$ in the following form:

$$\mathbf{z} \cdot \nabla \hat{G} = \left(z_s + z_n \frac{M_n M_s}{\beta_n^2} \right) \frac{\partial \hat{G}}{\partial s} + z_l \frac{\partial \hat{G}}{\partial l} + \frac{z_n}{\beta_n^2} \frac{\partial \hat{G}}{\partial \check{n}}$$

which extends to the whole surface S, the expression in Eq. (17) used on S_ε. As already observed above, the last term is weakly singular in $\mathbf{x}_0$ and thus in Eq. (22) it yields a convergent improper integral; the contribution from the tangential derivatives of $\hat{G}$ is a semiconvergent integral that depends on the shape of S_ε, and corresponds to their Cauchy principal value integral when S_ε is symmetric with respect to $\mathbf{x}_0$, as in our analysis.

Following this result, Eq. (5) has been determined observing that for the problem under examination $\mathbf{z} = -\rho_0 \mathbf{v} \cdot \mathbf{n}\mathbf{v} - p'_I \mathbf{n} - p'_B \mathbf{n} - \rho \mathbf{u}^- \cdot \mathbf{n}\mathbf{u}^+$. Note that in all the integral equations mentioned in this work, the integral terms containing a singular kernel have been developed as described in this appendix. Thus, although no symbolic reference to this fact is introduced, the resulting surface integrals have to be considered applied on $S \setminus S_\varepsilon$ in the limit as $\varepsilon \to 0$, i.e., with kernel singularity removed.

Appendix B. Comparison with an alternative approach

Let us introduce a stationary virtual closed surface, S, within a fluid region where an arbitrary unsteady pressure field, p', is present without being perturbed by any physical surface. Considering a point $\mathbf{x}$ in the field and neglecting second-order terms, Eq. (4) yields

$$0 = \int_S [\rho \dot{\mathbf{u}} \cdot \mathbf{n} \hat{G}]_{\text{ret}} \, dS + \int_S [p' \mathbf{n} \cdot \nabla \hat{G} - \dot{p}' \mathbf{n} \cdot \nabla \theta \hat{G}]_{\text{ret}} \, dS, \tag{23}$$

where $\mathbf{u}$ is the fluid velocity related to p' through the momentum equation. Eq. (23) is the compatibility condition on a closed surface between the pressure field and the corresponding velocity field, in an unbounded fluid medium. Then, if $p' \equiv p'_I$, $\mathbf{u} \equiv \mathbf{u}_I$ and the shape of S coincides with that of S_B, the combination of Eq. (23) with Eq. (4) written for an impermeable surface yields the following alternative boundary integral representation for the pressure scattered by a stationary surface:

$$4\pi p'_S(\mathbf{x}, t) = -\int_{S_B} \left[\frac{\rho \dot{\mathbf{u}}_I \cdot \mathbf{n}}{r} \right]_{\text{ret}} dS + \int_{S_B} \left[p'_S \frac{\mathbf{n} \cdot \mathbf{r}}{r^3} + \dot{p}'_S \frac{\mathbf{n} \cdot \mathbf{r}}{cr^2} \right]_{\text{ret}} dS \tag{24}$$

(note that, for the stationary surface, $\hat{G} = -1/4\pi r$). Observing that the linearized momentum equation gives $\rho \dot{\mathbf{u}}_I \cdot \mathbf{n} = -\partial p'_I / \partial n$, and using this expression in the equation above, one obtains that Eq. (24) coincides with Eq. (3) in Ref. [17]. This demonstrates the equivalence between the formulation presented here and that presented in Ref. [17] (note that in Eq. (3) of Ref. [17], $\cos\alpha = \mathbf{n} \cdot \mathbf{r}/r$). The difference between the two formulations is in the way in which the incident pressure forces the scattered one. In Ref. [17] this occurs through a term depending on its normal derivative on the scattering surface (similar to the formulations based on the Kirchhoff approach), whereas here the scattered pressure is forced by the distribution of the incident pressure and its time derivative on the same surface. Eq. (23) also shows that the term forcing the scattered pressure in the formulation examined here is closely related to the forcing term in the scattering formulations based on the velocity potential, which is given by the velocity flow related to the incident perturbation field.

References

[1] U. Iemma, M. Gennaretti, Integrated aeroacoustoelastic modeling for the analysis of the propeller-driven cabin noise, *AIAA Paper 99-1919*, *Fifth AIAA/CEAS Aeroacoustic Conference*, Bellevue, Washington, May 1999.
[2] C. Testa, S. Ianniello, G. Bernardini, M. Gennaretti, Sound scattered by a helicopter fuselage in descent flight condition, *AIAA Paper 2007-3497*, *13th AIAA/CEAS Aeroacoustics Conference*, Rome, Italy, May 2007.
[3] D. Colton, R. Kress, *Integral Equation Methods in Scattering Theory*, Wiley, New York, 1983.
[4] G.C. Gaunaurd, Elastic and acoustic resonance wave scattering, *Applied Mechanics Reviews* 42 (1989) 143–192.
[5] S. Amini, P.J. Harris, A comparison between various boundary integral formulation of the exterior acoustic problem, *Computational Methods in Applied Mechanics and Engineering* 84 (1990) 59–75.
[6] J.M. Gallman, M.K. Myers, F. Farassat, Boundary integral approach to the scattering of nonplanar acoustic waves by rigid bodies, *AIAA Journal* 29 (1991) 2038–2046.
[7] M.K. Myers, J.S. Hausmann, Computation of acoustic scattering from a moving rigid surface, *Journal of the Acoustical Society of America* 91 (1992) 2594–2605.
[8] P. di Francescantonio, The prediction of the sound scattered by moving bodies, *AIAA Paper 95-112*, *First AIAA/CEAS Aeroacoustics Conference*, Munich, Germany, May 1995.
[9] H.A. Schenck, Improved integral formulation for acoustic radiation problems, *Journal of the Acoustical Society of America* 44 (1968) 41–58.
[10] S. Amini, D.T. Wilton, An investigation on boundary element methods for the exterior acoustic problem, *Computational Methods in Applied Mechanics and Engineering* 54 (1986) 49–65.
[11] M. Gennaretti, A. Giordani, L. Morino, A third-order boundary element method for exterior acoustics with applications to scattering by rigid and elastic shells, *Journal of Sound and Vibration* 222 (1999) 699–722.
[12] M. Gennaretti, U. Iemma, Aeroacoustoelasticity in state-space format using CHIEF regularization, *Journal of Fluids and Structures* 17 (2003) 983–999.
[13] J.E. Ffowcs Williams, D.L. Hawkings, Sound generated by turbulence and surfaces in arbitrary motion, *Philosophical Transactions of the Royal Society A* 264 (1969) 321–342.
[14] M. Gennaretti, U. Iemma, C. Testa, Prediction of sound scattered by moving bodies with applications to propeller-driven airplanes, *AIAA Paper 2006-2475*, *12th AIAA/CEAS Aeroacoustic Conference*, Cambridge, MA, May 2006.
[15] A. Zinoviev, D.A. Bies, On acoustic radiation by a rigid object in a fluid flow, *Journal of Sound and Vibration* 269 (2004) 535–548.

[16] F. Farassat, Comments on the paper by Zinoviev and Bies, On acoustic radiation by a rigid object in a fluid flow, *Journal of Sound and Vibration* 281 (2005) 1217–1223.
[17] F. Farassat, M.K. Myers, Further comments on the paper by Zinoviev and Bies, On acoustic radiation by a rigid object in a fluid flow, *Journal of Sound and Vibration* 290 (2006) 538–547.
[18] A. Zinoviev, D.A. Bies, Author's reply, *Journal of Sound and Vibration* 290 (2006) 548–554.
[19] P. di Francescantonio, A new boundary integral formulation for the prediction of sound radiation, *Journal of Sound and Vibration* 202 (1997) 491–509.
[20] K.S. Brentner, F. Farassat, An analytical comparison of the acoustic analogy and Kirchhoff formulation for moving surfaces, *AIAA Journal* 36 (1998) 1379–1386.
[21] L. Morino, M. Gennaretti, Toward an integration of aerodynamics and aeroacoustics of rotors, *AIAA Paper 92-02003*, *DGLR/AIAA 14th Aeroacoustic Conference*, Aachen, Germany, May 1992.
[22] L. Morino, M. Gennaretti, Boundary integral equation methods for aerodynamics, in: S.N. Atluri (Ed.), *Computational Nonlinear Mechanics in Aerospace Engineering*, *Progress in Aeronautics and Astronautics*, Vol. 146, AIAA, Washington, DC, 1992, pp. 279–320.
[23] L. Morino, G. Bernardini, M. Gennaretti, A boundary element method for the aerodynamics and aeroacoustics of bodies in arbitrary motions, *International Journal of Aeroacoustics* 2 (2003) 129–156.
[24] F. Farassat, Derivation of formulations 1 and 1A of Farassat, NASA TM-2007-214853, 2007. (available at http://ntrs.nasa.gov/).
[25] F. Farassat, G.P. Succi, The prediction of helicopter rotor discrete frequency noise, *Vertica* 7 (1983) 309–320.
[26] K.S. Brentner, Prediction of helicopter rotor discrete frequency noise, NASA TM-87721, 1986.
[27] M. Gennaretti, Una formulazione integrale di contorno per la trattazione unificata di flussi aeronautici viscosi e potenziali, Ph.D. Dissertation, University of Rome 'La Sapienza', Rome, Italy, 1993 (in Italian).
[28] L.N. Long, The compressible aerodynamics of rotating blades based on an acoustic formulation, NASA TP-2197, 1983.
[29] F. Farassat, Quadrupole source in prediction of the noise of rotating blades—a new source description, *AIAA Paper 87-2675*, *11th AIAA Aeroacoustics Conference*, Sunnyvale, CA, October 1987.
[30] F. Farassat, K.S. Brentner, The uses and abuses of the acoustic analogy in helicopter rotor noise prediction, *Journal of the American Helicopter Society* 33 (1988) 29–36.
[31] S. Lee, K. Brentner, F. Farassat, Analytic formulation and numerical implementation of an acoustic pressure gradient prediction, *AIAA Paper 2007-3710*, *13th AIAA Aeroacoustics Conference*, Rome, Italy, May 2007.
[32] P.M. Morse, K.U. Ingard, *Theoretical Acoustics*, Princeton University Press, Princeton, 1987.
[33] A.D. Pierce, *Acoustics: An Introduction to Its Physical Principles and Applications*, Acoustical Society of America, New York, 1989.
[34] W.E. Baker, Axisymmetric modes of vibration of thin spherical shell, *Journal of Acoustical Society of America* 33 (1961) 1749–1758.
[35] M.C. Junger, Sound scattering by thin elastic shells, *Journal of Acoustical Society of America* 24 (1952) 366–373.
[36] X. Wu, A. Akay, Sound radiation from vibrating bodies in motion, *Journal of Acoustical Society of America* 91 (1992) 2544–2555.
[37] M. Tanaka, V. Sladek, J. Sladek, Regularization techniques applied to boundary element methods, *Applied Mechanics Reviews* 47 (1994) 457–499.
[38] R. Kress, *Linear Integral Equations*, Springer, Berlin, Heidelberg, 1989.
[39] L. Morino, A general theory of unsteady compressible potential aerodynamics, NASA CR-2464, 1974.